

ORIGINAL RESEARCH

# Optogenetic Control of Human Induced Pluripotent Stem Cell-Derived Cardiac Tissue Models

Amit Gruber , MD, PhD<sup>†</sup>; Oded Edri, MSc<sup>†</sup>; Shany Glatstein, MSc; Idit Goldfracht , PhD; Irit Huber, PhD; Gil Arbel, MSc; Amira Gepstein, PhD; Snizhanna Chorna, PhD; Lior Gepstein , MD, PhD

**BACKGROUND:** Optogenetics, using light-sensitive proteins, emerged as a unique experimental paradigm to modulate cardiac excitability. We aimed to develop high-resolution optogenetic approaches to modulate electrical activity in 2- and 3-dimensional cardiac tissue models derived from human induced pluripotent stem cell (hiPSC)-derived cardiomyocytes.

**METHODS AND RESULTS:** To establish light-controllable cardiac tissue models, opsin-carrying HEK293 cells, expressing the light-sensitive cationic-channel CoChR, were mixed with hiPSC-cardiomyocytes to generate 2-dimensional hiPSC-derived cardiac cell-sheets or 3-dimensional engineered heart tissues. Complex illumination patterns were designed with a high-resolution digital micro-mirror device. Optical mapping and force measurements were used to evaluate the tissues' electro-mechanical properties. The ability to optogenetically pace and shape the tissue's conduction properties was demonstrated by using single or multiple illumination stimulation sites, complex illumination patterns, or diffuse illumination. This allowed to establish in vitro models for optogenetic-based cardiac resynchronization therapy, where the electrical activation could be synchronized (hiPSC-derived cardiac cell-sheets and engineered heart tissue models) and contractile properties improved (engineered heart tissues). Next, reentrant activity (rotors) was induced in the hiPSC-derived cardiac cell-sheets and engineered heart tissue models through optogenetics programmed- or cross-field stimulations. Diffuse illumination protocols were then used to terminate arrhythmias, demonstrating the potential to study optogenetics cardioversion mechanisms and to identify optimal illumination parameters for arrhythmia termination.

**CONCLUSIONS:** By combining optogenetics and hiPSC technologies, light-controllable human cardiac tissue models could be established, in which tissue excitability can be modulated in a functional, reversible, and localized manner. This approach may bring a unique value for physiological/pathophysiological studies, for disease modeling, and for developing optogenetic-based cardiac pacing, resynchronization, and defibrillation approaches.

**Key Words:** arrhythmias ■ defibrillation ■ induced pluripotent stem cells ■ models ■ optical mapping ■ optogenetics ■ tissue engineering

Some of the hurdles in studying and developing better treatments for cardiac arrhythmias stem from the lack of suitable human cardiac tissue models, specifically those reflecting patient/disease-specific abnormalities, and from the inability to perform targeted, high-resolution, functional, and reversible perturbations of the system. The introduction

of 2 groundbreaking research methodologies: human induced pluripotent stem cells (hiPSC)<sup>1</sup> and optogenetics,<sup>2,3</sup> and their adaptation to cardiovascular research,<sup>4-6</sup> may allow to address the aforementioned challenges.

The advent of the hiPSC technology allowed establishing human in vitro patient-specific cardiomyocyte

Correspondence to: Lior Gepstein, MD, PhD, Rappaport Faculty of Medicine and Research Institute, Technion-Israel Institute of Technology, POB 9649, Haifa 3109601, Israel. E-mail: mdlior@technion.ac.il

<sup>†</sup>A. Gruber and O. Edri contributed equally to this article.

Supplementary Material for this article is available at <https://www.ahajournals.org/doi/suppl/10.1161/JAHA.121.021615>

For Sources of Funding and Disclosures, see page 18.

© 2022 The Authors. Published on behalf of the American Heart Association, Inc., by Wiley. This is an open access article under the terms of the Creative Commons Attribution-NonCommercial-NoDerivs License, which permits use and distribution in any medium, provided the original work is properly cited, the use is non-commercial and no modifications or adaptations are made.

JAHA is available at: [www.ahajournals.org/journal/jaha](http://www.ahajournals.org/journal/jaha)

## CLINICAL PERSPECTIVE

### What Is New?

- We combined human induced pluripotent stem cell-derived cardiomyocytes, tissue engineering, and optogenetic (light-sensitive channels and complex illumination) tools to generate 2- and 3-dimensional light-sensitive human cardiac tissue models of cardiac arrhythmias in which excitability can be perturbed in a controlled, functional, and reversible manner.
- Using this approach, we demonstrate the ability to synchronize electrical activity by optogenetic multisite pacing, resulting in improved mechanical function in the 3-dimensional engineered heart tissue model.
- Prolonged optogenetic stimulation was able to terminate reentrant arrhythmias in the 2-dimensional/3-dimensional models; defibrillation failure mechanisms involved too short or too long illumination durations.

### What Are the Clinical Implications?

- The experimental approaches described may materialize in the future into therapeutic interventions, including optogenetic-based pacing, resynchronization therapy, and reentrant arrhythmia termination.
- These experimental models generated could potentially be used to study the mechanisms underlying development of cardiac arrhythmia, successful optogenetic cardioversion and defibrillation failures.

### Nonstandard Abbreviations and Acronyms

<b>DMD</b>	digital micro-mirror device
<b>EHT</b>	engineered heart tissue
<b>hiPSC</b>	human induced pluripotent stem cell
<b>hiPSC-CCS</b>	hiPSC-derived cardiomyocyte cell-sheet
<b>hiPSC-CMs</b>	hiPSC-derived cardiomyocytes

tissue models. The generated hiPSC could be coaxed to differentiate into the cardiac lineage, yielding hiPSC-derived cardiomyocytes (hiPSC-CMs)<sup>7,8</sup> and even chamber-specific cardiomyocyte subtypes<sup>9–14</sup> from both healthy individuals<sup>7,8</sup> and patients with a variety of acquired<sup>15</sup> and inherited<sup>16–19</sup> cardiac disorders. The latter patient-specific hiPSCs-CMs were able to recapitulate the different disease phenotypes, to provide mechanistic insights into disease processes, and to serve as experimental platforms for drug testing.<sup>18</sup> More

recently, similar disease modeling and drug evaluation studies were also extended to the 2- and 3-dimensional tissue levels by combining hiPSC-CMs with tissue engineering strategies.<sup>14,20–23</sup> This allowed for the study of more complex electrophysiological processes such as conduction and reentrant arrhythmias.<sup>20,24–26</sup>

Optogenetics is an emerging discipline that uses optogenetic sensors and actuators for optical interrogation and control of excitable tissues.<sup>27</sup> The latter application involves the use of light-sensitive proteins (opsins), functioning as ion channels, ion pumps, or signaling receptors<sup>2,3,28</sup> for precise, localized, and low-energy optical control of excitable tissues such as the brain. By expressing opsins, like the depolarizing light-sensitive cationic channel ChR2 (Channelrhodopsin-2),<sup>29</sup> neuroscientists could develop the ability to selectively sensitized neurons to light, enabling precise perturbations of neural circuits. More recently, similar optogenetic tools were also applied in the cardiac research arena,<sup>4–6,30</sup> allowing to modulate cardiac excitability and to develop experimental optogenetic-based cardiac pacing,<sup>31,32</sup> resynchronization,<sup>30,32,33</sup> and defibrillation<sup>34–40</sup> strategies.

Recently, the combined use of optogenetic actuators and hiPSC-CMs have been described in the areas of drug testing and safety pharmacology (QT screening),<sup>41–43</sup> in hiPSC-CMs phenotypic studies, and for the induction of cell maturation.<sup>44</sup> Moreover, optogenetics was also applied in hiPSC-CMs based cardiac tissue engineering models to study the pathophysiological effects of chronic and intermittent tachy-pacing.<sup>45–47</sup>

Here, we aimed to combine the use of hiPSC-CMs and optogenetics tools for the derivation of 2- and 3-dimensional light-sensitive human cardiac tissues. By combining these in vitro models with the ability to apply complex illumination patterns in both space and time, we were able to establish unique approaches to visualize, perturb, and control cardiac tissue activity. These studies highlighted the potential of this approach to study reentrant arrhythmias and to model different optogenetic-based experimental therapies such as optogenetic pacing, resynchronization, and arrhythmia termination in relevant human cardiac tissues.

## METHODS

The data that support the findings of this study are available from the corresponding author upon reasonable request.

### Establishing the Engineered HEK293 Cells Expressing the Light-Sensitive Proteins

CoChR-expressing HEK293 cells were established using lentiviral transduction of the *CoChR-GFP* transgene (kindly provided by Ofer Yizhar, Weizmann

Institute). Briefly, the pLV-CAG-CoChR-GFP plasmid was used for virus production in 80% confluent HEK293T cells. The relevant plasmid was co-transfected with the packaging cassette NRF and the VSVG plasmid using PolyJet reagent (SignaGen-Laboratories); 8 µg DNA was used per 10 cm dish, where the transgene of interest, NRF, and VSVG plasmids were mixed in a 3:2:1 ratio. Fresh virus-containing media were collected at 48 and 72 hours and used for 2 rounds of infections. Transduced HEK293 cells were purified by 10-day G418 antibiotic (800 µg/mL) selection followed by eGFP (enhanced green fluorescent protein)-fluorescence based sorting using FACSAria (BD-Biosciences). CheRiff-expressing HEK293 cells were generated by Lipofectamine (Invitrogen)-based transfection of a pCDH-CMV-CheRiff-GFP plasmid. Transfected cells were purified using a combined G418 antibiotic (800 µg/mL, 10 days) and Fluorescence-activated cell sorting selection.

### hiPSCs Propagation and Cardiomyocyte Differentiation

Previously established hiPSCs<sup>15</sup> were used, which were generated based on the approval of Rambam Health Care Campus International Review Board (Helsinki) committee according to relevant guidelines and after obtaining relevant informed consent. Undifferentiated hiPSCs were propagated using mTeSR-1 medium. For cardiomyocyte differentiation, a modification of a monolayer directed differentiation system was used.<sup>48,49</sup> In brief, the differentiation Roswell Park Memorial Institute (RPMI) medium/B27 medium containing RPMI-1640, 2%-B27 supplement minus insulin (Life Technologies), 1% penicillin/streptomycin, and 6 mmol/L-CHIR-99021 (Stemgent) was used for 2 days. Medium was changed to RPMI/B27 (without CHIR) supplemented with 2 µmol/L-Wnt-C59 (Selleckchem) on days 3 and 4. Beating monolayers (20–60 days) were enzymatically dissociated into small-clusters or single-cells using TrypLE and used for co-cultures creation.

### Establishing Light-Responsive hiPSC-Derived Cardiac Cell-Sheet Co-Cultures

A modification of a recently-described large-scale (≈1 cm) circular-shaped hiPSC-derived cardiomyocyte cell sheet (hiPSC-CCS) model<sup>24</sup> was used for the current study.<sup>50</sup> Initially, 180 000 CoChR-HEK293 cells were seeded in the 10 mm inner-well of Matrigel-coated MatTet plate (P35G-1.5-10-C, MatTek) as a monolayer. Twenty-four hours later, seeded cells were treated with 24 µmol/L Mitomycin-C (Sigma) for 1 hour to prevent cell-proliferation. At day 2, 1×10<sup>6</sup> hiPSC-CMs were seeded on top of the CoChR-HEK293 monolayer to generate the co-cultures. After 12-to-14-hours, 2 mL

of fresh RPMI/B27 medium were added to the cultures with supplementation of 5 µmol/L Blebbistatin (B0560-5MG, Sigma) to prevent vigorous contraction. Experiments were conducted 3 to 5 days after seeding the hiPSC-CMs to allow formation of appropriate electrical coupling among the cells.

### Immunostaining

Cultures were fixed with 4% paraformaldehyde (Bio-Lab). Blocking was performed by 5% horse serum (Gibco, 1 hour). This was followed by overnight incubation (4 °C) with primary antibodies for connexin-43 (1:100; rabbit; Santa Cruz Biotechnology, sc-9059) and α-actinin (1:100; mouse; Sigma-Aldrich, A7811). Samples were washed (x3) with PBS and incubated (1 hour) with 1:150 diluted secondary antibodies: Cy3 donkey anti-mouse IgG (715-175-150, Jackson Immuno-research laboratories) and Cy5 donkey anti-rabbit IgG (711-175-152, Jackson). Antibodies were diluted in PBS with 3% horse-serum and 0.1% Triton. Nuclei were stained with DAPI (1:500, Sigma, D9564). Zeiss LSM-710 laser-scanning confocal microscope (Zeiss) was used for imaging.

### Optical Monitoring of the Tissue Models

Co-cultures were loaded with the voltage-sensitive dye Di4-ANBDQBS (22.5 µg/mL, acquired from Leslie Loew, University of Connecticut) for 15 minutes at room temperature. Blebbistatin (5 µM) was also added to the loading medium during the incubation period to prevent motion artifacts during optical mapping.<sup>24</sup> Optical mapping was performed using a macrocope (Olympus MVX10) equipped with a 1× objective (0.25 NA 6.3X - 63X MVPLAPO 1X, Olympus) and a high speed EM-CCD camera (Evolve-512 Delta, Photometrics) equipped with a chip of 512×512 pixels.<sup>24,25</sup> The field of view was 10×10 mm and acquisition was performed at 480 frames/sec and 8×8 binning. An exception was the defibrillation study in the hiPSC-CCSs, where 278 frames/sec and 8×8 binning were used.

The X-Cite Turbo LED-system served as light source. Excitation filter for Di4-ANBDQBS was Chroma ET620/60× and emission filter was Chroma ET665lp. The Micro-Manager software was used for data acquisition and the OMProCCD software (provided by Prof. Bum-Rak Choi, Brown University) served for analysis. Optical signals were analyzed to measure the local activation time (timing of maximal dF/dt signal) at each pixel and used to generate detailed activation maps. Filtration of the acquired optical signal data from the EM-CCD camera was performed using a spatial smoothing filter with a window of 3×3 pixels. Whenever calculation of activation time was needed, we used a spatial smooth filter with

a window of 11×11 pixels coupled with the use of an additional polynomial temporal filter that was applied on the raw data (third order, 13 points window size) and on the first derivative  $dF/dt$  (third order, 30 points window size).

### Optogenetic Illumination

Optical excitation was generated by a 470 nm centered LED (BLS-series High-Power Light Guide Coupled LED Source, Mightex Systems) equipped with a ET470/40× excitation filter and a T5851pxr dichroic mirror (Chroma-Technology). Patterned illumination protocols were generated by a digital micro-mirror device (DMD; Polygon-400, Mightex) controlled by PolyScan software.

Whenever light intensities are mentioned; they represent the measured light intensity at the sample.

### Generation of Engineered Heart Tissues

Engineered heart tissue (EHT) constructs were generated as described.<sup>20</sup> Briefly,  $2 \times 10^6$  hiPSC-CMs and  $1 \times 10^6$  Mitomycin-C treated engineered HEK293 cells were combined with bovine collagen (LLC Collagen-Solutions), 0.1 mol/L NaOH and 2×DMEM (containing 40% 5×DMEM, 40% fetal bovine serum, 15% H<sub>2</sub>O, 10 μL/mL glutamine, and 20 μL/mL penicillin/streptomycin). The mixture was pipetted into circular casting molds, where it solidified in a ring-shape. After 3 days, the tissue was transferred onto a silicon passive-stretcher. Medium (Iscove-Medium with 20% fetal bovine serum, 1% non-essential amino acids, 1% glutamine, 1% penicillin/streptomycin, and 100 μmol/L β-mercaptoethanol) was changed every other day. Electrical point-stimulation (5 milliseconds-long, 1 Hz) was used to pace the EHT with a stimulus isolation unit (SIU-102, Warner Ins.) and a platinum-iridium electrode (Alpha-Omega).

### Force Measurements

EHT-generated active forces were measured by the Aurora-Scientific's force-transducer and length controller (model 400A/322C). Measurements were made at 37°C in Tyrode solution after initial length standardization. Force and length signals were digitally recorded and analyzed using custom-written Matlab software. Filtration of the force traces and their first derivatives was performed using the Savitzky-Golay filter in Matlab with a polynomial order of 19. Finally, EHT cross-sectional area was measured for normalization.

### Statistical Analysis

Data are presented as mean±SEM. Statistical analysis was performed using GraphPad Prism or SPSS software. For studies comparing measurements (EHT forces or total activation time) from the same tissues at baseline and after intervention (diffuse

optogenetic illumination) we used paired Student *t*-test. Comparisons between different illumination patterns were analyzed using 1-way ANOVA for repeated measurements followed by post hoc Tukey test. For repeated measurements of binary variables (spiral wave induction/termination), data were presented as percentages.

A logistic model was specified to evaluate the combined effects of illumination pattern and duration on the probability of rotor termination that was based on 480 individual experiments performed. The dependent binary variable in the logistic model was rotor termination, with 2 independent variables of illumination pattern and illumination duration and illumination pattern-by-duration interaction (a significant interaction indicates that the slopes for odds of rotor termination by illumination time are significantly different across levels of illumination patterns). Robust clustered standard errors were used to adjust for within-experiment repeated measures. The results of the logistic regression model are presented as predicted probabilities of rotor termination. A value of  $P < 0.05$  was considered statistically significant.

## RESULTS

### Creation and Voltage-Clamp Characterization of Opsin-Carrying Engineered Cells

Opsin-donor cell-lines expressing the light-sensitive proteins were co-cultured with hiPSC-CMs to generate the 2- and 3-dimensional light-responsive human cardiac tissue models (Figure 1A). Specifically, we used stable HEK293 cell-lines that were engineered to express the potent channelrhodopsin variant CoChR. To confirm the presence of functional photocurrents in the engineered cells, we performed patch-clamp recordings from dispersed CoChR-expressing HEK293 cells (Figure 1B). These voltage-clamp recordings revealed negligible currents during darkness, whereas continuous blue-light illumination induced significant currents (Figure 1B). The resulting current-voltage curve, displaying peak and steady-state currents produced at different test potentials during illumination, is presented in Figure 1C. Notice the known inward rectification properties of the channelrhodopsin channel family with a reversal potential slightly  $> 0$  mV.

### Optogenetic Pacing in Light-Responsive Cell-Sheet Co-Cultures

Our first goal was to generate a 2-dimensional hiPSC-based cardiomyocyte tissue model that could be modulated by optogenetic interventions. To this end, we used a recently-described large-scale ( $\approx 1$  cm),

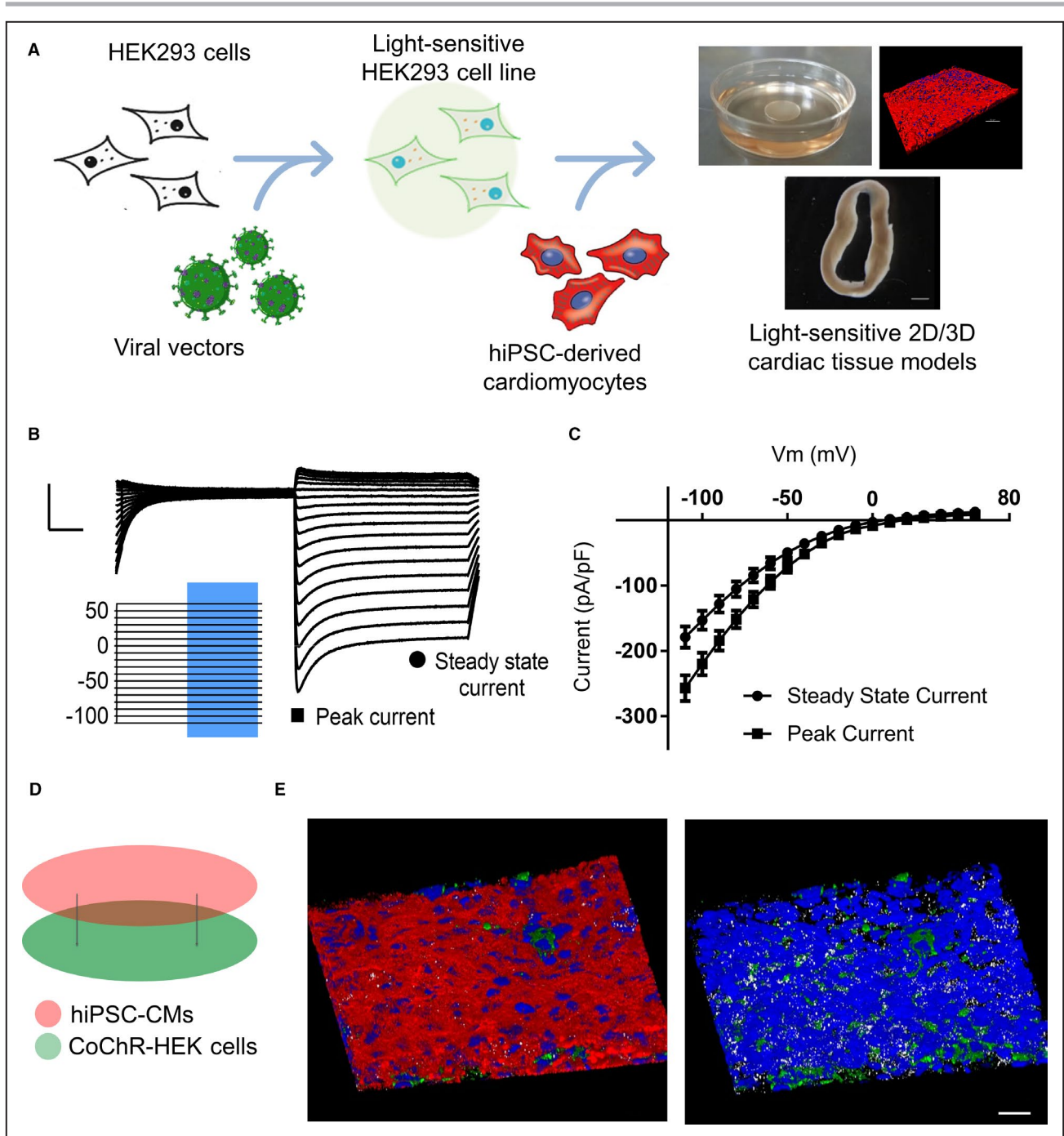


**Figure 1. Generation of light-sensitive cardiac tissue models.**

**A**, Scheme describing the generation of the light-sensitive human induced pluripotent stem cell-based cardiac tissue models. HEK293 cells were transduced to express the light-sensitive ion-channel CoChR and then seeded together with hiPSC-cardiomyocytes to form 2- or 3-dimensional light-sensitive cardiac tissue models. Voltage clamp recordings (**B**) and the corresponding current-voltage plot (**C**) showing robust light-induced CoChR photocurrents in the CoChR-HEK293 cells (n=5 cells). Shown are both peak and steady-state currents. **D**, Scheme describing the derivation of the in vitro co-culture model. The human induced pluripotent stem cell-cardiomyocyte cell sheets were seeded on top of a circular monolayer (diameter 1 cm) of CoChR-expressing HEK293 cells. **E**, Confocal microscopy 3D reconstructed z-series immunostainings of the co-cultures. The human induced pluripotent stem cell-cardiomyocytes are identified as  $\alpha$ -actinin positive cells (red) and engineered HEK293 cells by their eGFP expression (green). Gap junctions are indicated by the positive Cx43 punctuate immunosignal (white). Nuclei are counterstained with DAPI (blue). The right panel does not display the  $\alpha$ -actinin staining to better expose the underlying HEK cell layer and gap junction formation. Scale bar=20  $\mu$ m. hiPSC indicates human induced pluripotent stem cell; hiPSC-CMs, hiPSC-derived cardiomyocytes; and hiPSC-CCSs, hiPSC-derived cardiomyocyte cell sheets.

circular-shaped, hiPSC-derived cardiomyocyte cell-sheet (hiPSC-CCS) model.<sup>24</sup> To allow optogenetic control of the hiPSC-CCS, we seeded the layer of hiPSC-CMs on top of a layer of CoChR-expressing HEK293 cells (Figure 1D). Immunostaining analysis confirmed the co-existence of cardiomyocytes (alpha-actinin positive cells, red) with the engineered cells (eGFP expression) and the expression of the major gap-junction protein Cx43 between the cells (Figure 1E). As a result of the ability of HEK293 cells (similar to some other non-myocytes) to generate gap-junctions with neighbouring cardiomyocytes, as shown in the aforementioned immunostainings and in previous studies,<sup>6,30,51–54</sup> the resulting changes in their membrane potential attributable to the activation of the light-sensitive channels is hypothesized to modulate the electrophysiological properties of neighbouring cardiomyocytes through electrotonic interactions.

We next evaluated the ability of optogenetic stimulation to trigger electrical activity ("optogenetic pacing") in the generated co-cultures. To this end, we loaded the co-cultures with the voltage-sensitive dye, Di-4-ANBDQBS, and used a high-resolution optical mapping system<sup>24</sup> to monitor the tissues' electrical activity (Figure 2A and 2B). In addition to the 630 nm LED system used for voltage-sensitive dye excitation and optical mapping, the system also included a DMD that allows spatial patterning of 470 nm monochromatic light for optogenetic stimulation (Figure 2A).

The initial characterization of the light-sensitive co-culture model included the assessment of the efficacy of diffuse illumination flashes to capture and activate the co-cultures using different illumination conditions (Figure 2C through 2F). We first evaluated the effects of illumination rate by delivering the optogenetic flashes (duration: 1 millisecond, intensity: 0.16 mW/mm<sup>2</sup>) at different frequencies. As shown in Figure 2C, we were able to achieve 100% capture efficiency at pacing frequencies as fast as 2 Hz. The percentage of captured beats gradually decreased at faster stimulation frequencies.

We next performed dose-response studies, evaluating the effects of altering illumination intensity and duration (Figure 2D through 2F). Initially, we studied the

effects of varying light intensity at a fixed illumination duration (1 milliseconds, 1 Hz pacing) and noted that illumination intensities >0.08 mW/mm<sup>2</sup> resulted in 100% capture efficiency (Figure 2D). Similarly, dose-response curves were created by varying illumination durations at a fixed illumination intensity (0.1 mW/mm<sup>2</sup>, 1 Hz), which demonstrated that illumination durations >0.5 milliseconds resulted in 100% capture efficiency (Figure 2E). Finally, we derived strength-duration curves by varying both illumination intensity and duration and plotted the minimal set of paired values required to achieve 100% capture (Figure 2F).

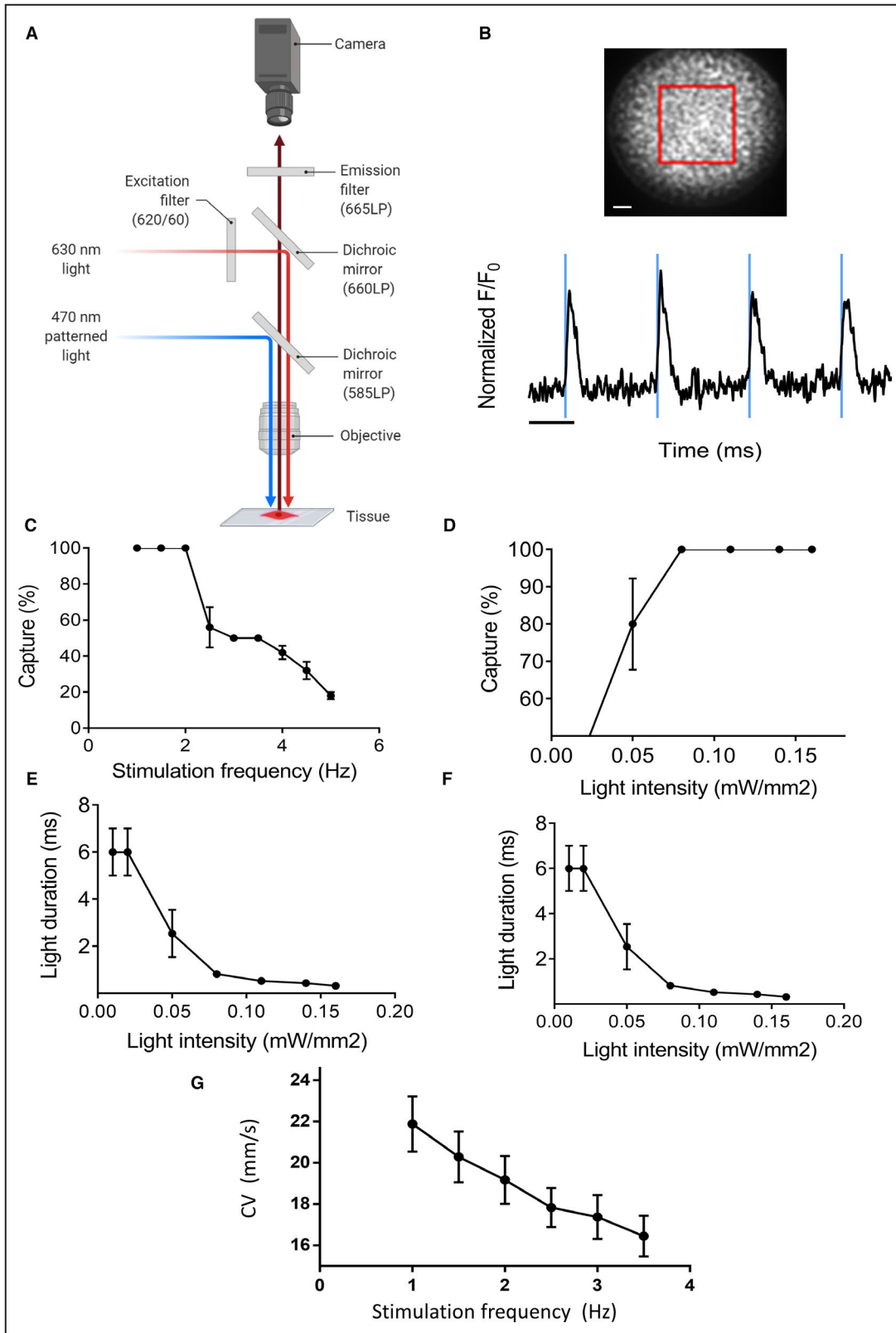
We also evaluated the conduction properties of the hiPSC-CCS co-cultures during optogenetic pacing. To this end, we used a point stimulation illumination protocol and optogenetically paced the cultures at different frequencies. Optical mapping was performed during optogenetic pacing and the resulting activation maps were analyzed to measure the average conduction velocity values at each pacing frequency. The resulting conduction velocity restitution plot is depicted in Figure 2G and shows the typical slowing of conduction with faster pacing rates.

## Optogenetic Pacing Patterns in the hiPSC-CCSs

We next aimed to develop an optogenetic approach that would allow generating complex activation patterns in the hiPSC-CCS co-cultures. To this end, we used the DMD to deliver illumination protocols that could be patterned in space and time (Figure 3A, top panel). Optical mapping was performed to characterize the resulting tissue activation patterns. As can be appreciated in Figure 3A (middle panel) the resulting tissue activation patterns closely correlated with the different applied DMD-based illumination patterns. Shown are activation maps derived during spontaneous activation (without illumination), during focal (single circular-site) or multi-site (4 circles) illuminations, using a linear illumination pattern, or during diffuse illumination. Notice that the origin of electrical activation was shaped exactly according to the patterned illumination, with the activation wavefronts then propagating

### Figure 2. Optogenetic pacing in the CoChR-HEK293/hiPSC-CCS co-culture model.

**A**, Schematic illustration of the EM-CCD based optical mapping and illumination systems. Arrows represent connection to different light sources, centred at 630 and 470 nm. **B**, Derivation of optical action potentials from the optical mapping recordings made from the hiPSC-CCSs during diffuse optogenetic pacing. Scale bars=1 mm and 500 milliseconds for the upper and lower panels, respectively. **C–F**, Optogenetic pacing capture-efficiency (n=5 hiPSC-CCSs). Mean capture rates are presented for diffuse light applications at different stimulation frequencies [using a fixed illumination duration (1 milliseconds) and intensity (0.16 mW/mm<sup>2</sup>)] (**C**); using different illumination intensities (each provided at a fixed 1 milliseconds duration and 1 Hz frequency) (**D**); and using different stimulation durations (at 1 Hz and a fixed 0.16 mW/mm<sup>2</sup> illumination intensity) (**E**). Also shown is the strength-duration curve, depicting the set of minimal paired amplitude-duration values necessary for 100% capture rate at 1 Hz frequency and different illumination intensities and duration (**F**). **G**, A restitution plot summarizing conduction velocity values measured from the hiPSC-CCS co-cultures during focal optogenetic pacing at different stimulation rates. Notice the typical slowing of conduction at faster pacing rates. CV indicates conduction velocity; and hiPSC-CCSs, human induced pluripotent stem cell-derived cardiomyocyte cell sheets.



to activate the non-illuminated areas (Figure 3A, middle-panel).

The total activation time of the hiPSC-CCs were measured and compared between the different

illumination patterns (Figure 3B). Notice that single site optogenetic pacing (using a focal circular illumination source) was associated with the longest total activation time (105±4 milliseconds, n=8). This setting

is analogous to the clinical situation of right-ventricular electrical pacing from a single site, which increases total left-ventricular activation time and leads to mechanical dyssynchrony. Multi-site activation of the

co-culture, originating simultaneously from 4 focal sites, significantly reduced the tissue activation time to  $75 \pm 4$  milliseconds ( $n=8$ ,  $P < 0.05$  compared with single-site pacing). Using a linear illumination pattern (a

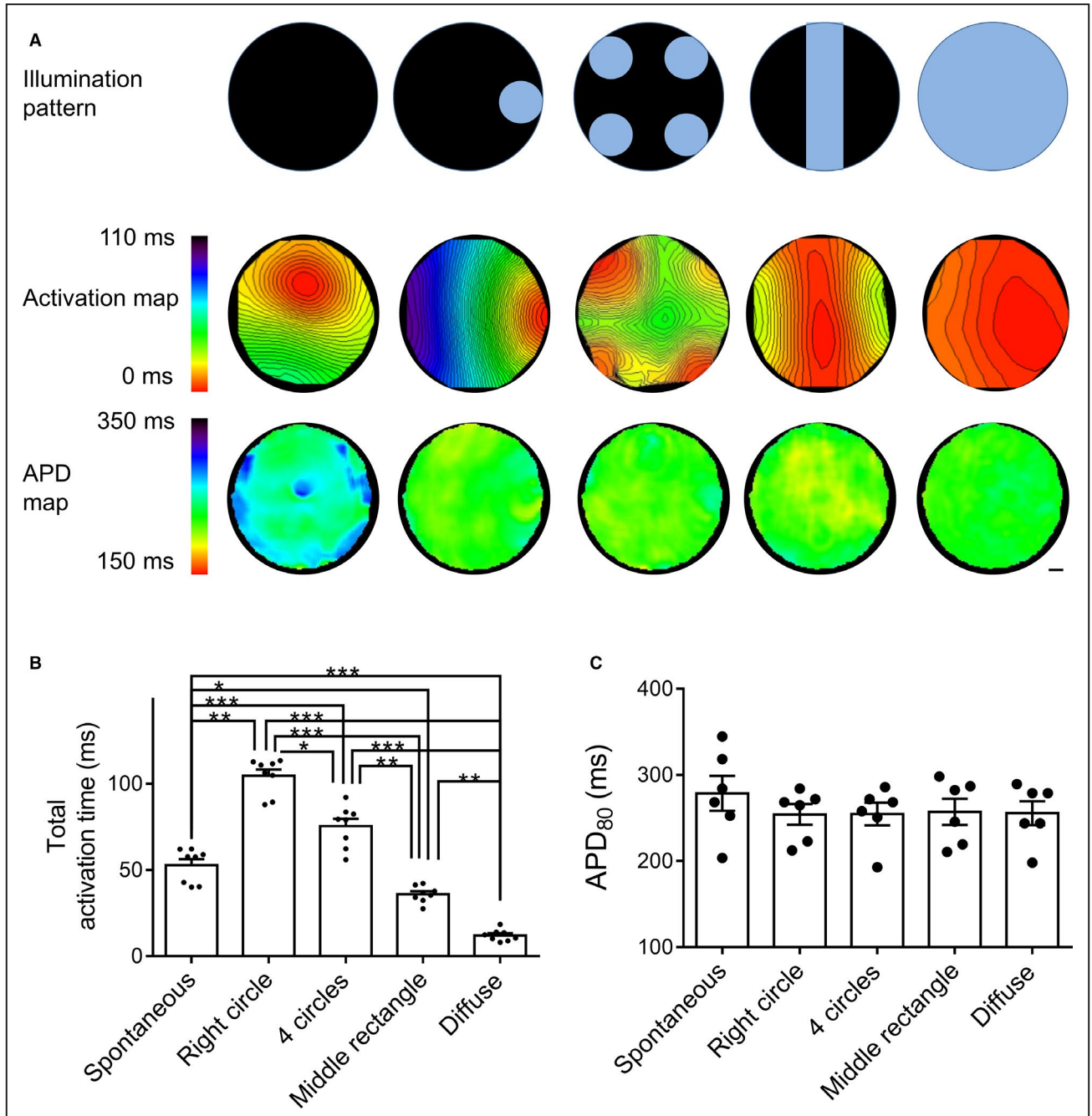


**Figure 3. Optogenetic pacing using complex illumination patterns.**

**A**, Optogenetic pacing in the hiPSC-CCSs using complex illumination patterns derived by the DMD. The top panel depict the different illumination patterns used for optogenetic pacing (no illumination, single circular focus, multi-site (4 circles), rectangular-shaped, and diffuse illumination). The middle and bottom panels show the resulting activation and APD<sub>80</sub> maps respectively, as constructed from the optical mapping results (isochrones, 5 milliseconds; scale bar=1 mm). Summary and statistical comparison of the measured total activation time (**B**) and APD<sub>80</sub> values (**C**), as a result of the different illumination patterns. Analysis was performed using 1-way ANOVA for repeated measurements followed by post hoc Tukey test ( $n=8$  and 6 hiPSC-CCSs for panels **B** and **C**, respectively). \* $P < 0.05$ . \*\* $P < 0.001$ . \*\*\* $P < 0.0001$ . APD<sub>80</sub> indicates action potential duration measured at 80% of repolarization; DMD, digital micro-mirror device; and hiPSC-CCSs, human induced pluripotent stem cell-derived cardiomyocyte cell sheets.

vertical rectangular at the center of the culture) further decreased total activation time to  $36\pm 2$  milliseconds ( $n=8$ ,  $P<0.001$  compared with the 4 focal activation sites). Finally, diffuse illumination synchronically activated the entire culture, resulting in the shortest total activation time ( $12\pm 1$  milliseconds,  $n=8$ ,  $P<0.001$  compared with all other stimulation protocols).

We also analyzed the effects of the different optogenetic pacing patterns on the repolarization properties of the tissues by generating action potential duration (APD) maps calculated at 80% of repolarization ( $APD_{80}$ , Figure 3A, bottom panel). No significant differences were noted in the  $APD_{80}$  values (Figure 3C) measured during optogenetic pacing at 1 Hz from a single site ("right-circle",  $254\pm 12$  milliseconds), from multiples sites ("4-circles",  $255\pm 13$  milliseconds), using a "middle-rectangular" illumination pattern ( $257\pm 15$  milliseconds), and using diffuse illumination ( $256\pm 14$  milliseconds). Note that the measured  $APD_{80}$  was slightly longer (but not statistically significant) during spontaneous rhythm without illumination ( $279\pm 20$ ), probably because of the slightly slower spontaneous beating rate.

### Optogenetics Pacing and Resynchronization in the EHT Model

After demonstrating that different optogenetic illumination designs can be used to modulate the hiPSC-CCS electrical activation patterns and to synchronize electrical activity, we next aimed to determine whether similar optogenetic resynchronization strategies can also affect the contractile properties of the tissue. To this end, we used a modification of the previously described 3-dimensional circular EHT model derived by embedding hiPSC-CMs within a collagen-based hydrogel.<sup>12,22</sup> To allow for optogenetic control of the EHT, we mixed during the process of EHT creation relatively purified cell-population of hiPSC-CMs (>80% cTnT<sup>+</sup> cells) with HEK293 cells expressing the ChR2 variant, CoChR (Figure 4A). The resulting EHTs were condensed as rings within casting molds and later transferred to a passive stretcher device, where they showed continuous contractions.

We next used our optical mapping system to examine the response of the EHT model to different optogenetic stimulation. In a similar manner to the characterization studies performed in the hiPSC-CCS co-culture model, we initially evaluated the effects of altering stimulation frequency, illumination intensity, illumination duration, and the intensity-duration relationship also in the EHT model (Figure 4B through 4E). As can be appreciated from the resulting plots (Figure 4B through 4E), a similar behavior to the hiPSC-CCS model was noted also in the EHT model with regards to all the illumination parameters studied.

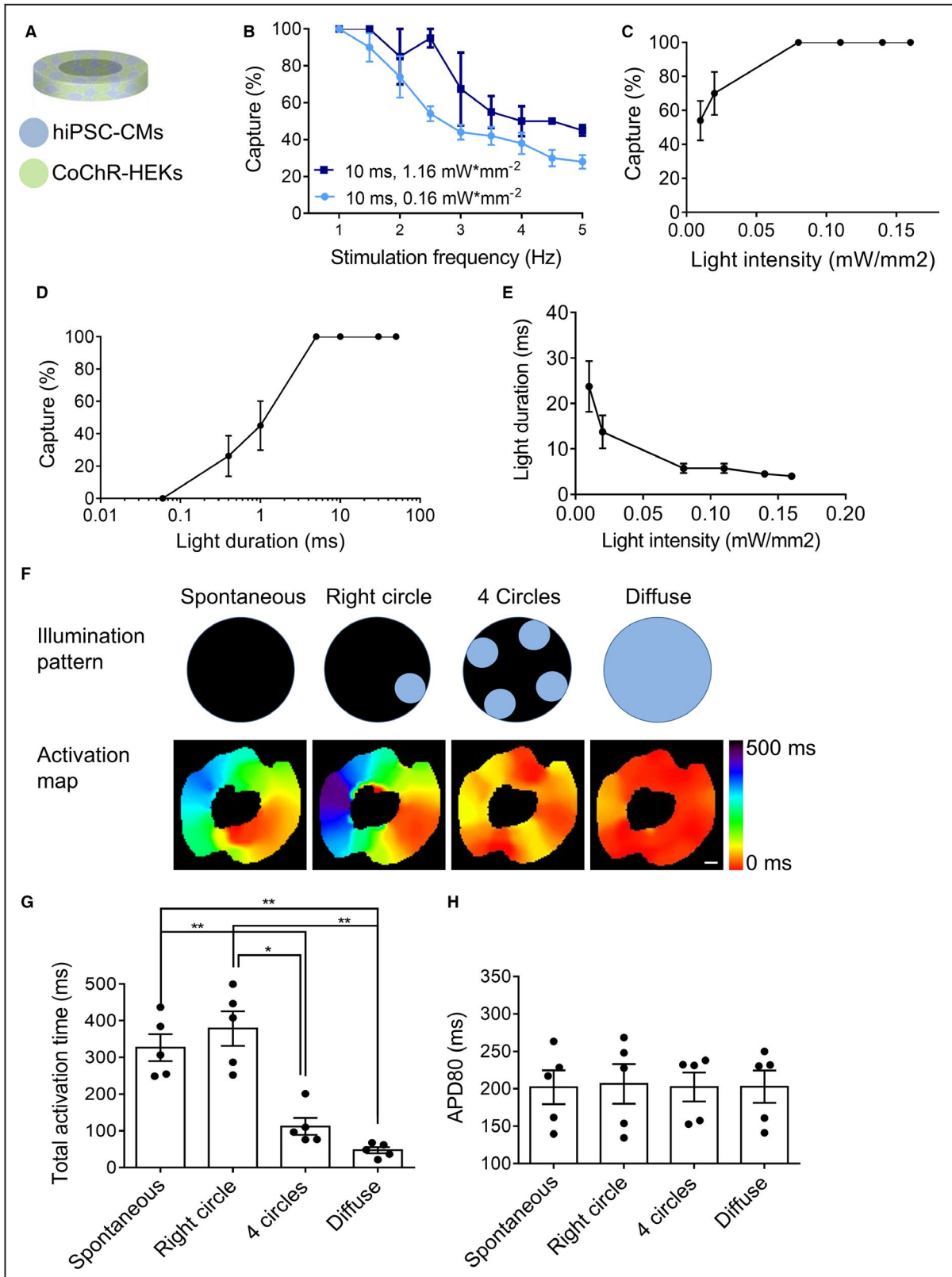
Next, we used the DMD apparatus to compare the effects of different illumination designs on the

activation patterns also in the EHT model (Figure 4F, top panel). The results of these studies are depicted as examples of the activation maps associated with each illumination pattern (Figure 4F, bottom panel) and in the quantitative summary plots of the specimens' total activation time (Figure 4G). Notice that both spontaneous activation and right-circle optogenetic pacing (both characterized by electrical activation spreading to activate the EHT from a single focus) were associated with the longest activation times, whereas the multi-site ("4-circles") and diffuse illumination pacing patterns were associated with the shortest total activation times. Finally, we also evaluated the effects of the different EHT optogenetic stimulation patterns on repolarization and noted that altering the pacing pattern did not significantly change  $APD_{80}$  values (Figure 4H).

Our next objective was to determine whether synchronizing electrical activity in the EHTs through optogenetic interventions can also affect the tissue's contractile properties. To this end, we used a sensitive force-transducer to study the mechanical properties of the ring-shaped EHT. Specifically, we compared the mechanical forces generated by the EHTs during point optogenetic stimulation to those resulting from diffuse EHT illumination (Figure 5A). As can be appreciated in the representative force measurement traces, diffuse illumination significantly improved the contraction properties of the tissue (Figure 5A). Force measurements from multiple EHTs revealed that diffuse illumination significantly increased the measured force amplitude ( $1.1\pm 0.1$  mN,  $n=10$ ,  $P<0.05$ , Figure 5B) as compared with focal illumination ( $0.9\pm 0.1$  mN). Similarly, maximal contraction velocity was increased from  $8.0\pm 0.8$  mN/ms to  $10.1\pm 0.8$  mN/ms ( $n=10$ ,  $P<0.001$ , Figure 5C) and maximal relaxation velocity was also improved from  $-6.0\pm 0.4$  mN/ms to  $-7.4\pm 0.5$  mN/ms ( $n=10$ ,  $P<0.01$ , Figure 5D) when comparing focal versus diffuse optogenetic stimulation. No significant changes were detected in the rise or decay times between focal and diffuse illumination ( $n=10$ , Figure 5E and 5F).

### Optogenetic Protocols to Induce Reentrant Arrhythmias

We next evaluated and compared the ability of different optogenetic protocols to induce reentrant arrhythmias in the CoChR-expressing hiPSC-CCS (CoChR-hiPSC-CCS) model. Initially, we compared 2 diffuse optogenetic illumination protocols: burst pacing versus the delivery of premature beats. In the burst pacing protocol, either 5, 10, or 15 repeats of diffuse 9 milliseconds-long illumination pulses were delivered at a pacing cycle length of 24 milliseconds. These optogenetic applications failed to induce arrhythmias in all attempts using 5 or 10 repeats and in 7 of 8 attempts involving 15 repeats.



Next, we evaluated the outcome of delivering premature stimulation using a diffuse S1 and S2 illumination protocol. As shown in Figure 6A and Video S1, application of a diffuse S2 optogenetic stimulation during a

specific time-interval could exploit intrinsic heterogeneities within the repolarizing tissue and trigger reentrant activity. Notice, in the color-coded representation of the fluorescent signal in Figure 6A, the spatial heterogeneities

**Figure 4. Optical pacing patterns in the hiPSC-derived engineered heart tissues (EHTs).**

**A**, Schematic illustration of the light-sensitive EHT model derived by mixing collagen, opsin-donor HEK293 cells, and hiPSC-CMs. **B–E**, Capture-efficiency of optogenetic pacing. Mean capture rates are presented for 10 milliseconds-long diffuse illuminations at different stimulation frequencies and intensities (**B**, n=5 and 4 EHTs for experiments done with 0.16 and 1.16 mW\*mm<sup>-2</sup> light intensities, respectively); using different intensities at a fixed 10 milliseconds duration and 1 Hz frequency (**C**, n=5 EHTs); and using different stimulation durations at 1 Hz and a fixed 0.16 mW/mm<sup>2</sup> illumination intensity (**D**, n=8 EHTs). The strength-duration curve, depicting the minimal illumination duration necessary for 100% capture rate at different illumination intensities, is also shown (**E**, n=8 EHTs). **F**, Optogenetic pacing in the EHTs using complex illumination patterns. Examples of activation maps generated during optogenetic pacing using single-site (“Right circle”), multi-site (“4-circles”) and diffuse illumination, as compared with an activation map generated during spontaneous rhythm (no illumination). **G–H**, Quantitative summary of the total activation time (**G**) and APD<sub>80</sub> values (**H**) measured during the different illumination patterns. Analysis was performed using one-way ANOVA for repeated measurements followed by post hoc Tukey test. n=5 EHTs (\*P<0.05, \*\*P<0.01). APD<sub>80</sub>: action potential duration measured at 80% of repolarization; EHT, engineered heart tissue; hiPSC, human induced pluripotent stem cell; and hiPSC-CMs, hiPSC-derived cardiomyocytes.

in the membrane potential developing during the S1-related repolarizing phase (t=48–94 milliseconds). Such repolarization heterogeneities resulted in development

of areas of functional conduction block following delivery of the S2 diffuse illumination, leading to initiation of reentrant activity with multiple cores of spiral waves

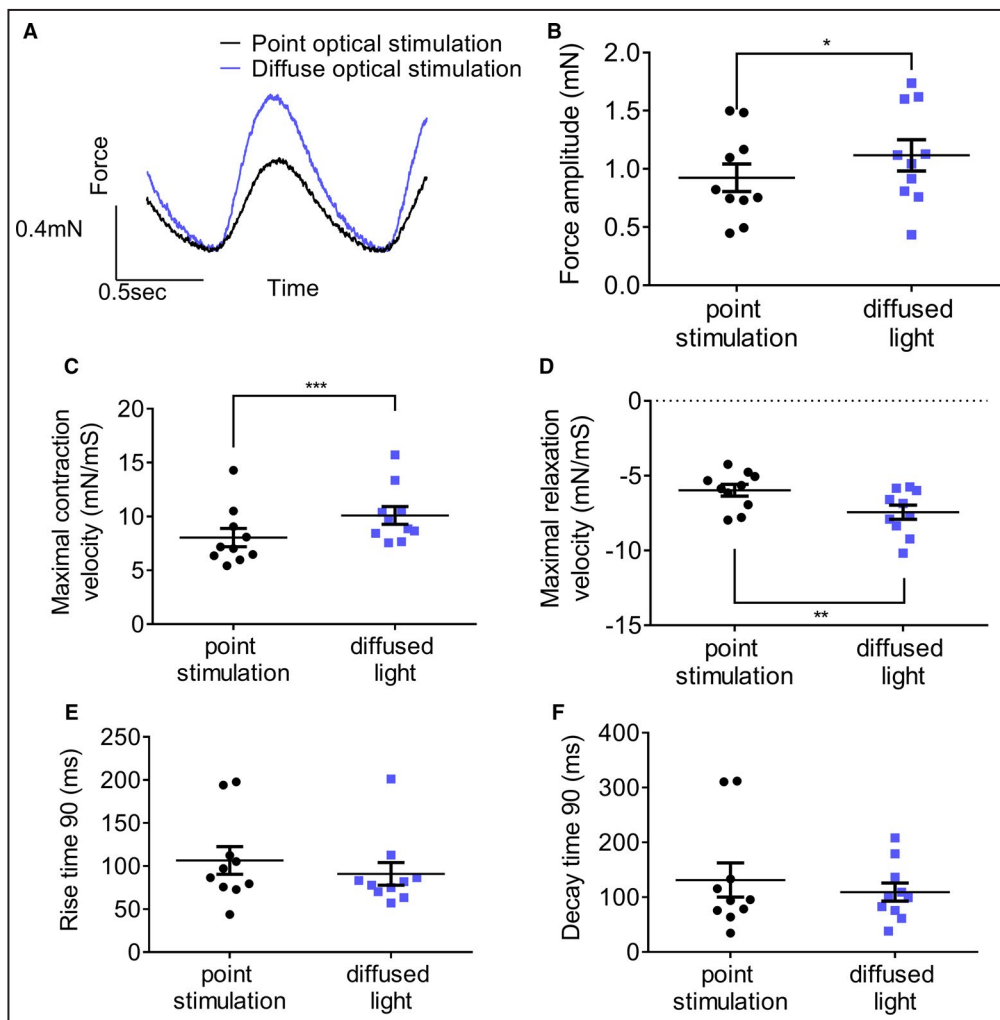
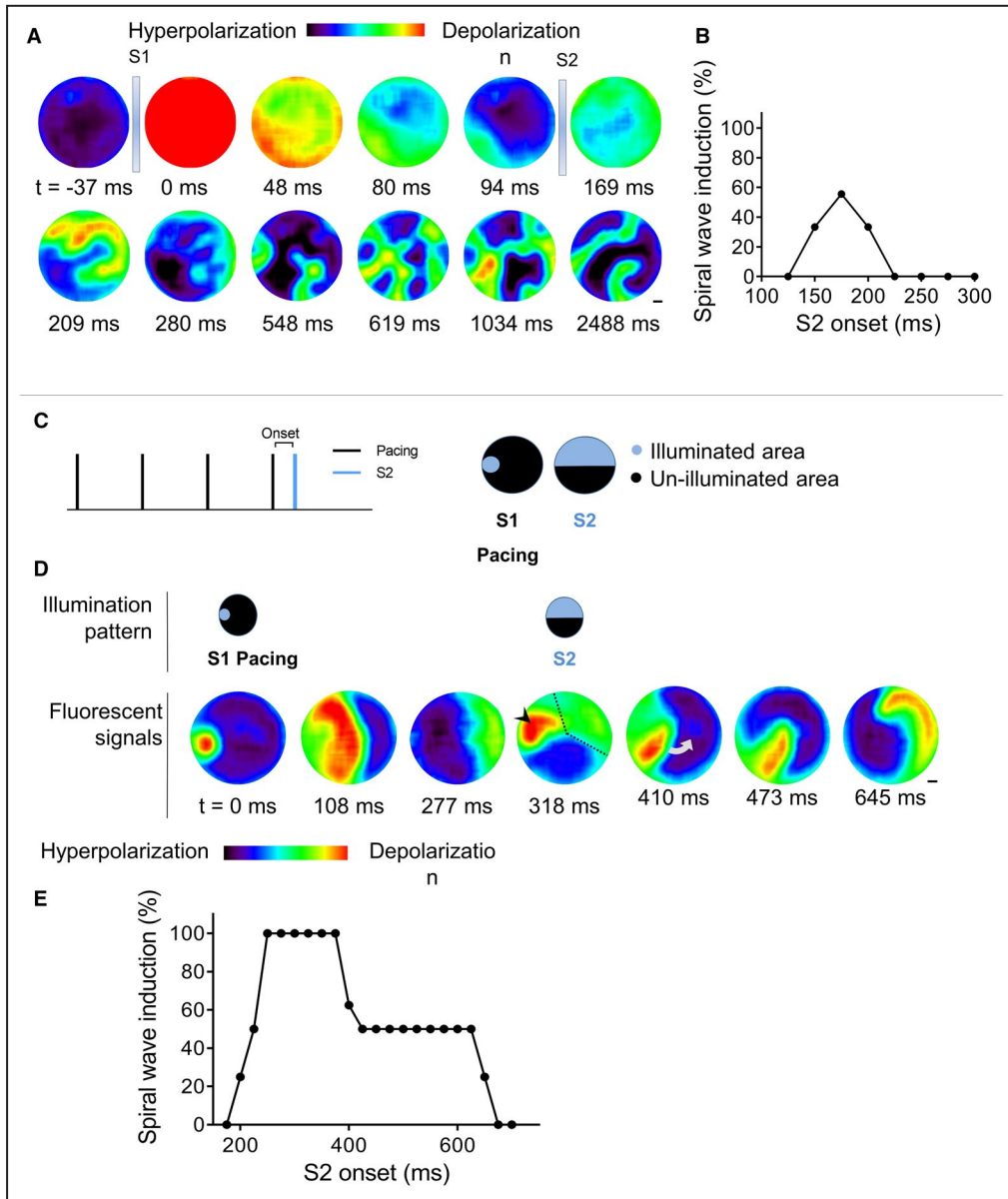


**Figure 5. Engineered heart tissue force measurements during focal and diffuse optogenetic stimulations.**

**A**, Representative force measurements traces from the engineered heart tissue, as measured during point and diffuse optogenetics stimulations. Scale bars=0.4 mN and 0.5 seconds. **B** through **F**, Summary of the different parameters quantifying the mechanical forces measurements during point and diffuse light stimulations. Summarized are force amplitude (**B**); maximal contraction (**C**) and maximal relaxation (**D**) velocities; and rise (**E**) and decay (**F**) times. (n=10 engineered heart tissues, \*P<0.05, \*\*P<0.01, \*\*\*P<0.001). EHT indicates engineered heart tissue.



( $t=209$  milliseconds and onwards in Figure 6A and Video S1). We next systematically evaluated the effects of S2 timing (by altering S1 and S2 interval) on the tissue's arrhythmia vulnerability (Figure 6B). Interestingly, only S2 onsets between 150 and 200 milliseconds could trigger arrhythmias, with a peak efficiency of 55.6% with a S2 onset of 175 milliseconds ( $n=9$ , Figure 6B).

Finally, to achieve a more robust and uniform approach for arrhythmia induction, we combined our CoChR-hiPSC-CCS co-culture model with a cross-field stimulation strategy<sup>55,56</sup> used to generate reentry in different cardiac-tissue models. Here, we converted the traditional electrical-based cross-field stimulation strategy into an optogenetic-based protocol<sup>56</sup> that is schematically outlined in both time and space in Figure 6C. An example of how a reentrant activity is induced by the optogenetic

cross-field stimulation protocol in the CoChR-HEK293-hiPSC-CCSs co-cultures can be viewed by the optical mapping results, presented either as a dynamic display (Video S2) or by sequential fluorescent images (Figure 6D). Notice that the co-culture is initially optogenetically paced using a point stimulation (S1) originating from the left-side of the culture. When the S1-induced wavefront reaches the center of the tissue, a perpendicular wavefront is initiated by a broad S2 optogenetic-based stimulation wave originating from the top of the culture. The S2 propagating wave then impinges on the tale of the S1 activation-wave, initiating spiral-wave reentry.

Using the aforementioned conditions, we were able to generate sustained reentrant activity (spiral waves) reproducibly in all the CoChR-hiPSC-CCS co-cultures studied ( $n=8$ ; Figure 6D through 6E and Video S2). We

**Figure 6. Induction of spiral waves in the human induced pluripotent stem cell-derived cardiomyocyte cell sheets (hiPSC-CCSs).**

**A and B,** Spiral wave induction by a diffuse Stimulation 1 (S1) and Stimulation 2 (S2) premature stimulation protocol. **A,** Shown are sequential fluorescent snapshots taken from the dynamic display of the optical mapping results. The color spectrum depicts the fluorescence levels of the tissue, which correlated with relative changes in membrane potential (purple represents hyperpolarized tissue while red represents depolarized tissue). The timing of the diffuse S1 and S2 stimulation is marked by the light blue rectangles. Note the depolarization throughout the tissue (red) induced immediately after application of the diffuse S1 optogenetic stimulation ( $t=0$ ). This was followed eventually by the repolarization process (48–94 milliseconds). Delivery of the S2 diffuse illumination during the repolarization period resulted in the development of functional conduction blocks within the tissue ( $t=209$ ) that lead to the development of spiral waves ( $t=280$ – $2488$  milliseconds). Scale bar=1 mm. **B,** Statistical analysis of the incidence of spiral wave induction as function of the time interval between S1 and S2 (“S2 onset”). ( $n=9$  hiPSC-CCSs). **C through E,** Optogenetic cross-field protocol to induce spiral waves in the hiPSC-CCSs. **C,** Schemes describing the cross-field optogenetic stimulation protocols used to induce reentry in both time (left) and space (right). **D,** Fluorescence time-lapse snapshots of a representative hiPSC-CCSs during cross-field optogenetic stimulation. The co-culture is optogenetically paced using a point stimulation (S1,  $t=0$ ) from the left-side of the culture. When the S1-induced wavefront reaches the center of the tissue, a perpendicular wavefront is delivered by a broad S2 optogenetic-based stimulation wave originating from the top half of the culture (S2,  $t=318$  milliseconds). This new wavefront is able to pre-excite the already excitable tissue proximal to the traveling S1 wave (318 milliseconds, marked by the arrowhead) and initiate a sustained spiral-wave (410–645 milliseconds). Scale bar=1 mm. **E,** Summary of the spiral wave induction rates as function of the timing of S2 onset. ( $n=8$  hiPSC-CCSs). hiPSC-CCSs indicates human induced pluripotent stem cell-derived cardiomyocyte cell sheets.

next evaluated the effects of the timing of S2 delivery in the optogenetic cross-field stimulation strategy on arrhythmia induction rate. In contrast to the optogenetic premature stimulation protocol where the time-window for arrhythmia induction was narrow (Figure 6B), the time window for spiral wave induction using the optogenetic cross-field stimulation protocol was relatively wide (Figure 6E). Consequentially, we observed a 100% arrhythmia induction rate when using an S2 onset of 250 to 375 milliseconds and >50% induction rate with an S2 onset of 250 to 650 milliseconds.

### Optogenetic Protocols to Terminate Reentrant Arrhythmias

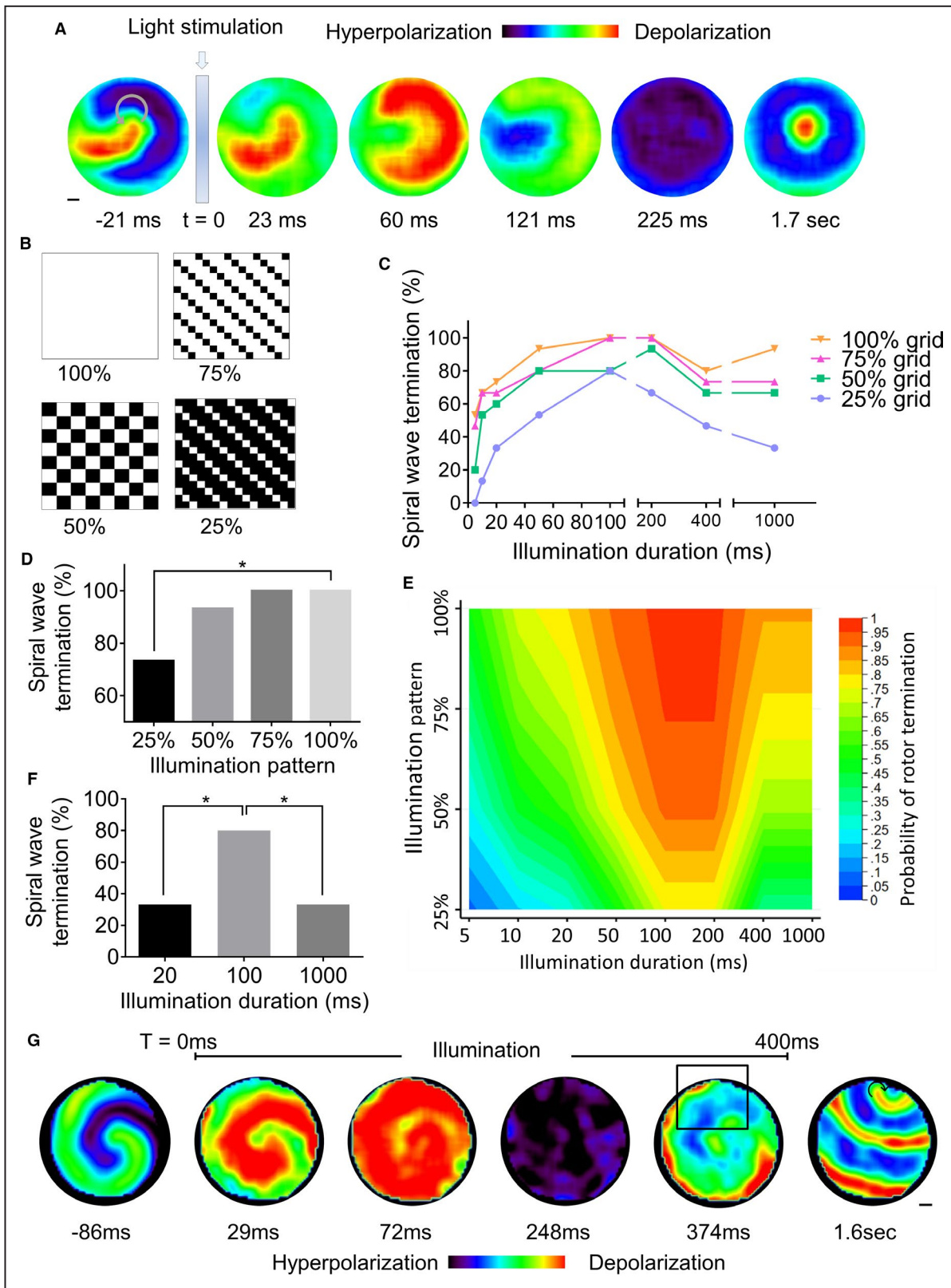
Following establishment of a reproducible optogenetic-based approach to induce reentrant arrhythmias in the hiPSC-CCSs, we next aimed to evaluate the ability of optogenetic interventions to terminate such spiral waves. To this end, we applied continuous illumination in a diffuse manner to the co-cultures and were able to successfully terminate the arrhythmogenic activity (Figure 7A and Video S3). The mechanism underlying termination of rotor activity was related to the illumination-induced depolarization that occurred when large areas in the tissue were in a relatively hyperpolarized (excitable) state at the moment of light delivery (Figure 7A at  $t=23$ – $60$  m and Video S3). The illumination-related depolarization prevented further spiral-wave propagation, eventually leading to its termination (Figure 7A,  $t=60$ – $225$  milliseconds) and resumption of spontaneous focal activity (Figure 7A,  $t=1.7$  seconds).

We next aimed to minimize the illumination area required for arrhythmia termination by designing diffuse illumination patterns in which different percentages of the visual field (100%, 75%, 50%, and 25% illumination areas) are exposed to light (Figure 7B). Figure 7C

summarizes the success rate of each illumination pattern in arrhythmia termination as well as the effects of altering illumination durations at each illumination grid. Notice that maximal termination rates for all illumination patterns were observed when using illumination durations of 100 to 200 milliseconds. Focusing on the optimal illumination duration (200 milliseconds) we noted that while 100% illumination area resulted in the highest conversion rate (100%), using 75% or 50% illumination grids were associated with similar termination rates (100% and 93%, respectively, Figure 7D,  $n=15$ ). Interestingly, even when using a 25% illumination grid, although associated with statistically significant lower termination rates ( $P<0.05$ ), a 200 milliseconds illumination-duration protocol still resulted in 67% efficacy.

Based on the 480 individual experiments performed in the aforementioned studies, we developed a statistical model to predict arrhythmia termination probability as a function of the illumination parameters (duration and pattern) used. The model was constructed using logistic regression and the predicted probability of rotor termination is presented as a contour color plot (Figure 7E). Examining the model, we identified a few interesting observations. First, we noticed the existence of an optimal “defibrillation time-window”, in which maximal termination rate of spiral waves could be achieved (yellow/orange/red areas representing arrhythmia termination probabilities  $>0.75$ ).

Second, it became apparent that using optimal illumination durations for arrhythmia termination was especially important when using illumination grids with lower-densities (25%–50%). For example, for achieving a termination success rate  $>75\%$  one would need to apply a narrow range of illumination durations (100–200 milliseconds) at an illumination grid of 25%, whereas when using a 100% illumination grid any illumination duration  $>15$  milliseconds (15–1000 milliseconds) would



achieve similar success rates. The greater dependency on using optimal illumination durations at lower illumination grids was also shown statistically. In the logistic model, there was a strong grid-by-illumination duration

interaction ( $P=0.007$ ), which indicates that the slopes of rotor termination probability to the illumination duration is significantly different for the 4 different illumination grids studied (Figure S1). Notice that the rate of

**Figure 7. Optogenetic spiral wave termination in the human induced pluripotent stem cell-derived cardiomyocyte cell sheets (hiPSC-CCS) model.**

**A**, Optical mapping derived fluorescence time-lapse snapshots of a representative response to a diffuse illumination protocol aiming to terminate reentry in a hiPSC-CCS with ongoing spiral wave activity ( $t=-21$  milliseconds). The timing of the 20 milliseconds-long diffuse light stimulation is marked by a light-blue rectangle ( $t=0$ ). The color spectrum depicts the relative changes in membrane potential (purple represents hyperpolarized tissue while red represents depolarized tissue). Note that the diffuse illumination caused depolarization of the tissue that was in a resting, hyperpolarized state, at the time of the optogenetic stimulation ( $t=23-60$  milliseconds). The resulting depolarization led to termination of the spiral wave ( $t=121-225$  milliseconds) and to resumption of spontaneous focal pacemaker activity ( $t=1.7$  seconds). **B**, Illustration of the different illumination patterns used to minimize the illumination area required for arrhythmia termination. **C**, Summary of spiral wave termination rates, using the different illumination patterns, as function of illumination duration. ( $n=15$  hiPSC-CCSs). **D**, Comparison of the arrhythmia termination rate among the different illumination grids using an illumination duration of 200 milliseconds. ( $n=15$  hiPSC-CCSs,  $*P<0.05$  using Cochran Q test with Dunn post hoc comparisons). **E**, Contour plot showing the probability of rotor termination according to the illumination duration and illumination pattern. Predicted probabilities of rotor termination were calculated using logistic regression based on 480 experiments at different illumination durations and patterns. **F**, Comparison of the arrhythmia termination rate using illumination durations of either 20, 100, or 1000 milliseconds, in the 25% illumination grid. ( $n=15$  hiPSC-CCSs,  $*P<0.05$  using Cochran Q test with Dunn post hoc comparisons). **G**, Mechanism of optogenetic defibrillation failure following prolonged illumination. Shown are optical mapping derived fluorescence time-lapse snapshots obtained before, during, and after a prolonged illumination protocol in a hiPSC-CCS with an ongoing spiral wave activity ( $t=-86$  milliseconds). Note the initial depolarization of the non-excited tissue ( $t=29$  milliseconds) that leads to successful rotor termination ( $t=72-248$  milliseconds). This was followed by development of depolarization in a narrow rim at the periphery of the culture ( $t=374$  milliseconds) that led to the induction of a new reentrant circuit ( $t=1.6$  seconds) at an area that displayed increased local heterogeneity in membrane potentials (box in  $t=374$  milliseconds). hiPSC-CCSs indicates human induced pluripotent stem cell-derived cardiomyocyte cell sheets.

the increase in the probability of rotor termination with the change in illumination duration (slope of the lines in Figure S1) progressively decreases moving from a grid of 25% to 100% grid. A steeper slope, characterizing the 25% grid, indicates a larger dependency of rotor termination on the illumination duration. By contrast, the

near-horizontal slope of the 100% grid indicates minimal dependency on illumination duration for achieving rotor termination.

The third interesting and somewhat surprising finding was that not only short illumination durations ( $\leq 50$  milliseconds) were less effective in terminating

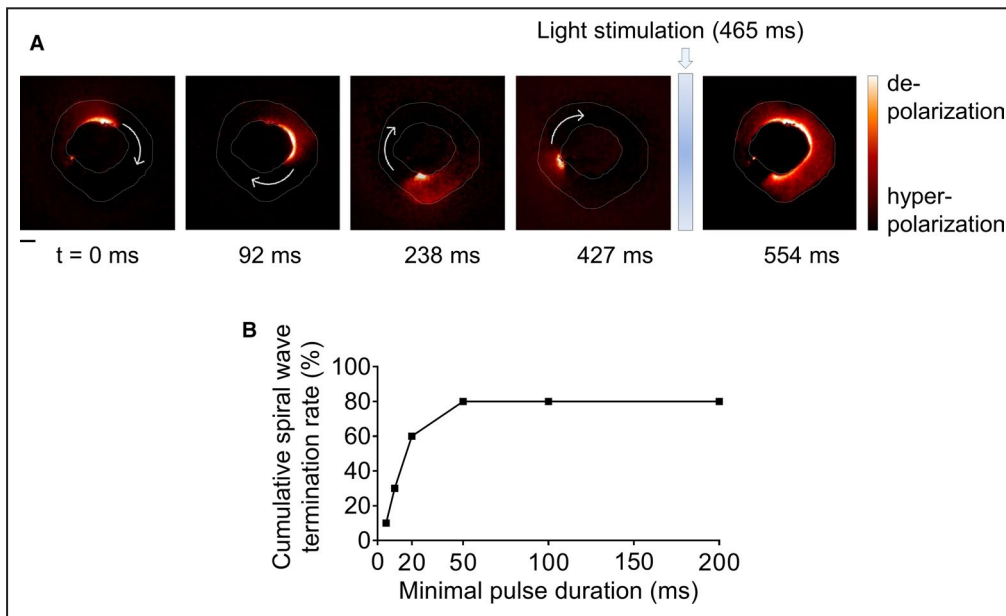


**Figure 8. Reentrant wave termination by optogenetic illumination in the engineered heart tissue model.**

**A**, Fluorescence time-lapse snapshots of a representative response to a diffuse light stimulation in the CheRiff-expressing engineered heart tissue with an ongoing macro-reentrant circuit ( $t=0-427$  milliseconds). The available excitable tissue is stimulated by a 10 milliseconds-long light stimulation (marked by a light blue rectangle,  $t=465$  milliseconds). Note that the resulting depolarization stops the perpetuating reentrant wave ( $t=554$  milliseconds). Dashed line indicates the margins of the engineered heart tissue. Arrows indicate the direction of propagation. Scale bar=1 mm. **B**, Summary of the cumulative reentry wave termination rates as function of illumination duration ( $n=10$  engineered heart tissues). EHT indicates engineered heart tissue.

reentry, but also long illumination durations ( $\geq 400$  milliseconds) were associated with reduced efficacy. Note for example the significantly higher arrhythmia termination rate at 100 milliseconds illumination duration (80%) as compared with both 1000 milliseconds illumination (33% termination rate,  $P < 0.05$ ) and 20 milliseconds illumination (33% termination rate,  $P < 0.05$ ) when using the 25% illumination grid (Figure 7F).

We next aimed to decipher the mechanism underlying the optical “defibrillation” failures in our model. While it is relatively easy to appreciate why too short illuminations may fail to terminate arrhythmias, it is less trivial to understand why long illumination durations also display reduced success rates. To provide insights into the latter phenomenon, we performed detailed optical mapping experiments of the hiPSC-CCSs during prolonged illuminations. As exemplified in the sequential fluorescent images in Figure 7G and in Video S4, the prolonged illumination signal was initially successful in terminating the spiral wave in the hiPSC-CCS model by inducing diffuse tissue depolarization followed by hyperpolarization (time: 29–248 milliseconds). Nevertheless, the continuous illumination then induced a new and relatively thin area of depolarization at the periphery of the tissue ( $t = 374$  milliseconds, red), which resulted in the development of a new propagating wavefront that then initiates a continuous reentrant circuit ( $t = 374$  milliseconds to 1.6 seconds) propagating around the area characterized by significant local heterogeneity in the membrane potentials ( $t = 374$  milliseconds, box).

### Terminating Arrhythmias in the EHT Model

Finally, we also evaluated the ability to terminate reentrant activity also in the 3-dimensional EHT model containing HEK293 cells that express an alternative ChR2 variant, CheRiff. Following induction of reentrant activity in the circular light-sensitive EHT model using burst electrical pacing, we delivered a diffuse optogenetic stimulation to the tissue (Figure 8A). This resulted in depolarization of the non-depolarized EHT tissue at the time of illumination (Figure 8A, 465–554 milliseconds). The resulting depolarization prevented the propagation of the reentrant wavefront, leading to termination of the arrhythmia. We next evaluated the effect of prolonging the optogenetic stimulation duration on the cumulative reentry termination rate and noted a plateau at 50 milliseconds in which 80% of the arrhythmic events were terminated (Figure 8B,  $n = 10$ ).

## DISCUSSION

We combined the groundbreaking optogenetics and hiPSC technologies to establish light-responsive in vitro human cardiac tissue models, whose electrical

properties could be remotely modulated at a high spatiotemporal resolution and in a functional and reversible manner. Specifically, our results revealed: (1) the ability to combine 2-dimensional (hiPSC-CCS) and 3-dimensional (EHT) hiPSC-based cardiac tissue models, opsin delivery cells, and an illumination apparatus (DMD) to establish unique light-sensitive human cardiac tissue models that can be used for several applications; (2) the ability to induce complex optogenetic pacing designs and variable conduction patterns in the hiPSC-based cardiac tissue models from a single focus, from multiple sites, using complex illumination patterns, and using diffuse illumination; (3) the ability of the optogenetic-based “cardiac resynchronization therapy” strategy in the EHT model to improve the tissue’s contractile properties; (4) the ability to utilize different optogenetic strategies to induce reentrant activity in the hiPSC-derived cardiac tissue models, with the cross-field stimulation protocol being the most effective; and (5) the ability to use optogenetic protocols to terminate reentrant activity in these models, to provide insights into arrhythmia termination successes and failures, and to determine the critical illumination parameters required for arrhythmia cessation.

The combined use of hiPSC-CMs and optogenetics has been reported recently in a number of studies focusing primarily at the cellular level in the areas of drug testing and safety pharmacology (facilitating studies investigating drug effects on action-potential duration) including as part of automated high throughput all-optical platforms,<sup>41–43</sup> as a novel non-invasive approach for voltage-clamp like studies to assess drug effects on ionic currents,<sup>57</sup> for hiPSC-CMs phenotyping, and as a way to induce cardiomyocyte maturation.<sup>44,58</sup> More recent studies also described the use of optogenetic pacing in hiPSC-based cardiac tissue models to allow modeling of catecholaminergic polymorphic ventricular tachycardia<sup>59</sup> and to evaluate the pathophysiological effects of chronic tachy-pacing, revealing significant tissue remodeling and increased susceptibility to arrhythmias.<sup>45</sup> Here, we utilized hiPSC-derived 2- and 3-dimensional engineered cardiac tissues as unique experimental models to evaluate potential optogenetic-based therapies; namely optogenetic pacing, resynchronization (“optogenetic cardiac resynchronization therapy”) and arrhythmia termination (“optogenetic defibrillation/cardioversion”) strategies.

By using opsin-expressing engineered cells, capable of generating gap junctions with neighboring cardiomyocytes,<sup>6,30,51,52</sup> we were able to optogenetically pace the hiPSC-CCSs and EHTs. We used this method as an alternative approach to direct gene delivery because of 2 reasons. First, we wanted to demonstrate and facilitate the concept of engraftment of genetically-modified opsin-carrying cells as a future optogenetic therapeutic strategy. Such a combined cell and gene

therapy approach has several potential advantages, including the ability to characterize and control the translation profile of the chosen transgene prior to cell delivery, the avoidance from the use of viral vectors with their potential side effects, and the potential beneficial effects of the transplanted cells themselves (for example when using cardiomyocyte precursor cells). Second, the hiPSC-CCS/HEK co-culture approach can be used to test different opsins in a robust, easy, and well-defined manner. The alternative approach of directly expressing the chosen opsin in the hiPSC-CCS in an efficient and homogenous manner, either by viral transduction of the hiPSC-CMs or by generating stable genetically-modified hiPSC lines expressing the light-sensitive proteins, has been extremely difficult to achieve.

Optogenetic pacing displayed both a characteristic frequency-response curve (allowing 100% capture efficiency for up to 2 Hz with 1 milliseconds-long optical stimulations) as well as typical dose-response curves (100% capture at illumination intensities and durations above 0.08 mW/mm<sup>2</sup> and 0.4 milliseconds respectively). While most previously described in-vitro and in-vivo optogenetic pacing studies used single-site or diffused pacing we were able, in this study, to use the DMD apparatus to derive complex illumination patterns that allowed to activate the tissues with variable and pre-determined conduction patterns. One application of this approach is the ability to study the effects of different conduction patterns, in both space and time, on the tissue electrophysiological properties and arrhythmogenesis.

A second application of the aforementioned approach is the ability to study the role of different conduction patterns on the tissue mechanical properties and specifically to design novel optogenetics-based cardiac resynchronization therapy strategies. We have recently demonstrated the ability to significantly shorten left-ventricular total activation time in the isolated rat heart model using multi-site (3 or 4 sites) optogenetic pacing.<sup>32</sup> Multi-site optogenetic pacing was made possible by distinct delivery of the AAV-ChR2 vector to a number of left-ventricular sites followed by targeted or diffuse illumination to simultaneously activate these sites. Here, we used an alternative approach in which CoChR is expressed diffusely throughout the tissue and the different pacing/conduction patterns are achieved by using different illumination designs. Using this approach in the EHT model, we were able to demonstrate that synchronous optogenetic activation of the entire EHT resulted in improved contractile performance in comparison with single-site pacing, with the latter setting mimicking the clinical scenario of ventricular desynchronization. Improvement in the EHT mechanical function was manifested both by an increase in the measured force amplitude as well as in the maximal contraction and relaxation velocities.

We next demonstrated the potential of the light-sensitive hiPSC-derived tissue models to study the processes involved in both the induction and termination of reentrant arrhythmias. Initially, we evaluated 3 types of optogenetic-based arrhythmia induction protocols in the hiPSC-CCS model: burst pacing, the delivery of premature stimulations, and a cross-field stimulation protocol. These studies revealed the limited ability of burst pacing to induce arrhythmias in the hiPSC-CCS model with most conditions tested failing to initiate reentry. The delivery of diffuse premature optogenetic stimulation (S2), taking advantage of the spatial repolarization heterogeneities that develop in the post-S1 repolarization phase, displayed a higher success rate in inducing reentrant arrhythmias (up to ~55%). The time window of the S2 coupling interval that could induce reentry, however, was rather narrow (150–200 milliseconds). The most effective approach for arrhythmia induction was the optogenetic cross-field stimulation protocol.<sup>56</sup> This optogenetic variation of the electrical cross-field stimulation strategy<sup>55</sup> allowed to robustly and reproducibly induce reentrant activity (spiral-waves) in all co-cultures. Interestingly, the time window during which the perpendicular S2-induced wavefront could generate reentry was rather wide (250–650 milliseconds).

In the last part of the study, we evaluated and characterized the ability to use optogenetic strategies for arrhythmia termination in the hiPSC-CCS and EHT models. Similar to previous in vitro (primary rat cardiomyocyte cultures)<sup>56,60</sup> and in vivo (mouse and rat hearts)<sup>34–38</sup> optogenetic defibrillation/cardioversion approaches, we used prolonged light activation of ChR2-derivatives to achieve continuous depolarization diffusely throughout our in vitro human cardiac tissue arrhythmia models. This approach resulted in robust arrhythmia termination in both the hiPSC-CCS and EHT models.

We also evaluated the optimal range of illumination parameters (illumination duration and the minimal illumination area density [critical mass]) required for arrhythmia termination in the hiPSC-CCS model. An optimal illumination duration (100–200 milliseconds) was identified in which the probability for successful arrhythmia termination was high not only when using the 100% illumination grid but also when using lower illumination densities (75%, 50%, and 25%). These results may have implications both to the mechanisms underlying arrhythmia termination and to the ability to minimize energy requirements for future optogenetic defibrillation strategies.

With regards to stimulation duration, we identified an optimal time window for "optogenetic defibrillation" that resulted in maximal arrhythmia termination efficacy. Interestingly, this optimal illumination duration time window was much narrower when using the lower-density illumination protocols. The mechanism

for the reduced success rate outside this optimal time-frame differs between the ‘too short’ and ‘too long’ stimulation durations. Short illumination durations ( $\leq 50$  milliseconds) were probably not sufficient to allow long enough durations of localized conduction block for arrhythmia termination. In contrast, long illumination durations ( $\geq 400$  milliseconds), while successfully terminating the original reentrant circuits, were associated with the induction of new action-potentials because of the continuous illumination related depolarization, which could then initiate new reentrant activity.

Arrhythmia termination by optogenetic-related depolarization can potentially stem from 2 underlying mechanisms.<sup>38</sup> According to the first mechanism, continuous illumination creates large areas of local functional conduction block, which prevents existing traveling wavelets from further propagation and therefore leads to their extinction. The second mechanism involves induction of  $\geq 1$  additional excitation wavefronts from areas that are in the excitable gap. These new wavefronts can then collide with the re-entrant wave and force its termination. While the former mechanism requires relative prolonged depolarization the latter strategy requires relatively short illumination (to trigger new action-potentials) and the presence of a relatively wide excitable gap.

While we cannot rule out that the induction of new excitation waves plays some role in the mechanism underlying arrhythmia termination in our model (especially in the EHT model where the anatomical reentry results in a large excitable gap), it seems that the functional conduction block is the prevailing mechanism. Evidence supporting this conclusion relates to the fact that we did not identify “real” action-potential propagation following illumination, probably because of the homogeneous and synchronous depolarization achieved. In addition, both short illumination durations and reduced density of the illuminated area were less effective in terminating arrhythmias. Since illumination protocols using shorter durations or lower density grids are still hypothesized to trigger action-potentials in areas that are in the excitable gap, the reduced arrhythmia termination efficiency associated with these modified interventions highly suggests that the colliding wave termination hypothesis is probably not the main underlying mechanism.

Finally, the cell-based gene delivery approach used in our study is not without limitations. First, to limit proliferation of the HEK293 cells we pretreated these cells with mitomycin. This raises a question on how the size of the cell-graft will change, in both the in vitro and in vivo settings, if mitomycin is not used. Importantly, because of their oncogenic properties, HEK293 cells will probably not be used clinically. Consequentially, characterization of other cell types that can be genetically modified and grafted as opsin-carrier cells such as cardiac fibroblasts, fibroblasts from other tissue sources, Mesenchymal stem cells, and human pluripotent stem

cell-derived cardiomyocytes may be more clinically relevant. However, such cells may behave differently from HEK cells with regards to their proliferative and engraftment properties, their active and passive electrical properties, their interaction profile with host cardiomyocytes including different electrotonic coupling properties, and their ability to induce potential paracrine effects.

In summary, we describe the combined usage of the emerging technologies of hiPSC-CMs, tissue engineering, and optogenetics together with a controllable light-emitting apparatus to derive light-sensitive in vitro human cardiac tissue models. This allowed to visualize, perturb, and control the electrophysiological activity in these human cardiac tissue model with high spatial and temporal resolutions. Our studies also highlighted the potential of these models to contribute to the mechanistic understanding of reentrant arrhythmias and for modeling different optogenetic-based experimental therapies such as optogenetic pacing, electromechanical resynchronization, and reentrant arrhythmia termination.

## ARTICLE INFORMATION

Received March 21, 2021; accepted December 21, 2021.

### Affiliations

Sohnis Research Laboratory for Cardiac Electrophysiology and Regenerative Medicine, The Rappaport Faculty of Medicine and Research Institute, Technion–Israel Institute of Technology, Haifa, Israel (A. Gruber, O.E., S.G., I.G., I.H., G.A., A. Gepstein, S.C., L.G.); and Cardiology Department, Rambam Health Care Campus, Haifa, Israel (L.G.).

### Sources of Funding

This study was funded by the European Research Council (ERC-2017-COG-773181-IPS-ChOp-AF), by the Israel Science Foundation (grant no. 1088/18), and by the Crown Foundation.

### Disclosures

None.

### Supplementary Material

Figure S1

Videos S1–S4 Legends

## REFERENCES

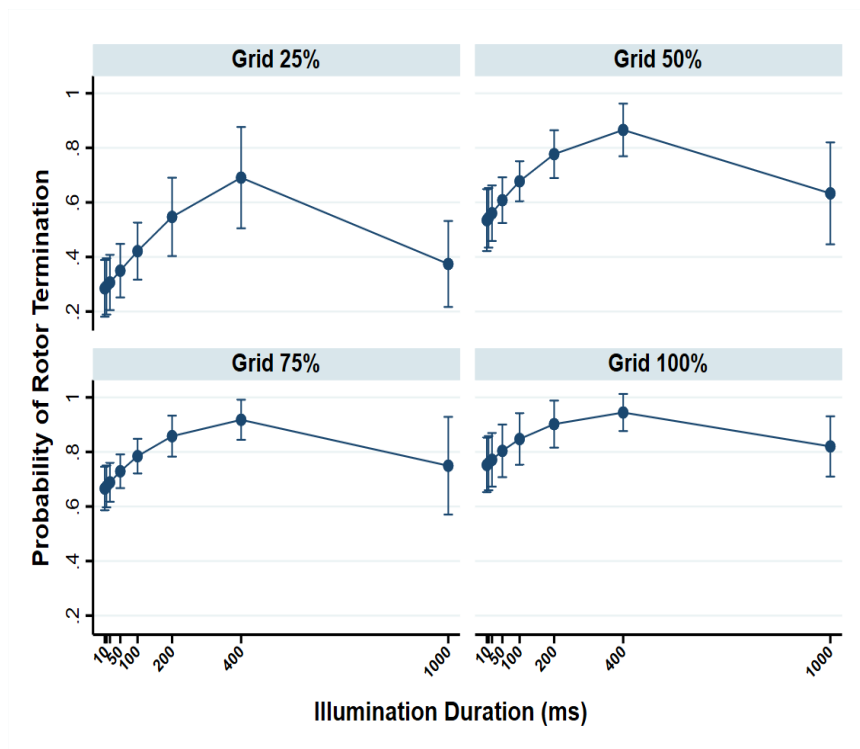
1. Takahashi K, Tanabe K, Ohnuki M, Narita M, Ichisaka T, Tomoda K, Yamanaka S. Induction of pluripotent stem cells from adult human fibroblasts by defined factors. *Cell*. 2007;131:861–872. doi: 10.1016/j.cell.2007.11.019
2. Boyden ES, Zhang F, Bamberg E, Nagel G, Deisseroth K. Millisecond-timescale, genetically targeted optical control of neural activity. *Nat Neurosci*. 2005;8:1263–1268. doi: 10.1038/nn1525
3. Deisseroth K. Optogenetics: 10 years of microbial opsins in neuroscience. *Nat Neurosci*. 2015;18:1213–1225. doi: 10.1038/nn.4091
4. Arrenberg AB, Stainier DY, Baier H, Huisken J. Optogenetic control of cardiac function. *Science*. 2010;330:971–974. doi: 10.1126/science.1195929
5. Bruegmann T, Malan D, Hesse M, Beiert T, Fuegemann CJ, Fleischmann BK, Sasse P. Optogenetic control of heart muscle in vitro and in vivo. *Nat Methods*. 2010;7:897–900. doi: 10.1038/nmeth.1512
6. Jia Z, Valiunas V, Lu Z, Bien H, Liu H, Wang HZ, Rosati B, Brink PR, Cohen IS, Entcheva E. Stimulating cardiac muscle by light: cardiac optogenetics by cell delivery. *Circ Arrhythm Electrophysiol*. 2011;4:753–760. doi: 10.1161/CIRCEP.111.964247

7. Zhang J, Wilson GF, Soerens AG, Koonce CH, Yu J, Palecek SP, Thomson JA, Kamp TJ. Functional cardiomyocytes derived from human induced pluripotent stem cells. *Circ Res*. 2009;104:e30–e41. doi: 10.1161/CIRCRESAHA.108.192237
8. Zwi L, Caspi O, Arbel G, Huber I, Gepstein A, Park IH, Gepstein L. Cardiomyocyte differentiation of human induced pluripotent stem cells. *Circulation*. 2009;120:1513–1523. doi: 10.1161/CIRCULATIONAHA.109.868885
9. Bjork S, Ojala EA, Nordstrom T, Ahola A, Lijestrom M, Hyttinen J, Kankuri E, Mervaala E. Evaluation of optogenetic electrophysiology tools in human stem cell-derived cardiomyocytes. *Front Physiol*. 2017;8:884. doi: 10.3389/fphys.2017.00884
10. Devalla HD, Schwach V, Ford JW, Milnes JT, El-Haou S, Jackson C, Gkatzis K, Elliott DA, Chuvá de Sousa Lopes SM, Mummery CL, et al. Atrial-like cardiomyocytes from human pluripotent stem cells are a robust preclinical model for assessing atrial-selective pharmacology. *EMBO Mol Med*. 2015;7:394–410. doi: 10.15252/emmm.201404757
11. Protze SI, Liu J, Nussinovitch U, Ohana L, Backx PH, Gepstein L, Keller GM. Sinoatrial node cardiomyocytes derived from human pluripotent stem cells function as a biological pacemaker. *Nat Biotechnol*. 2017;35:56–68. doi: 10.1038/nbt.3745
12. Goldfracht I, Protze S, Shiti A, Setter N, Gruber A, Shaheen N, Nartiss Y, Keller G, Gepstein L. Generating ring-shaped engineered heart tissues from ventricular and atrial human pluripotent stem cell-derived cardiomyocytes. *Nat Commun*. 2020;11:75. doi: 10.1038/s41467-019-13868-x
13. Lee JH, Protze SI, Laksman Z, Backx PH, Keller GM. Human pluripotent stem cell-derived atrial and ventricular cardiomyocytes develop from distinct mesoderm populations. *Cell Stem Cell*. 2017;21:179–194.e4. doi: 10.1016/j.stem.2017.07.003
14. Lemme M, Ulmer BM, Lemoine MD, Zech ATL, Flenner F, Ravens U, Reichenspurner H, Rol-Garcia M, Smith G, Hansen A, et al. Atrial-like engineered heart tissue: an in vitro model of the human atrium. *Stem Cell Rep*. 2018;11:1378–1390. doi: 10.1016/j.stemcr.2018.10.008
15. Zwi-Dantsis L, Huber I, Habib M, Winterstern A, Gepstein A, Arbel G, Gepstein L. Derivation and cardiomyocyte differentiation of induced pluripotent stem cells from heart failure patients. *Eur Heart J*. 2013;34:1575–1586. doi: 10.1093/eurheartj/ehs096
16. Moretti A, Bellin M, Welling A, Jung CB, Lam JT, Bott-Flügel L, Dorn T, Goedel A, Höhnke C, Hofmann F, et al. Patient-specific induced pluripotent stem-cell models for long-QT syndrome. *N Engl J Med*. 2010;363:1397–1409. doi: 10.1056/NEJMoa0908679
17. Sun N, Yazawa M, Liu J, Han L, Sanchez-Freire V, Abilez OJ, Navarrete EG, Hu S, Wang LI, Lee A, et al. Patient-specific induced pluripotent stem cells as a model for familial dilated cardiomyopathy. *Sci Transl Med*. 2012;4:130ra147. doi: 10.1126/scitranslmed.3003552
18. Matsa E, Ahrens JH, Wu JC. Human induced pluripotent stem cells as a platform for personalized and precision cardiovascular medicine. *Physiol Rev*. 2016;96:1093–1126. doi: 10.1152/physrev.00036.2015
19. Itzhaki I, Maizels L, Huber I, Zwi-Dantsis L, Caspi O, Winterstern A, Feldman O, Gepstein A, Arbel G, Hammerman H, et al. Modelling the long QT syndrome with induced pluripotent stem cells. *Nature*. 2011;471:225–229. doi: 10.1038/nature09747
20. Goldfracht I, Efrain Y, Shinnawi R, Kovalev E, Huber I, Gepstein A, Arbel G, Shaheen N, Tiburcy M, Zimmermann WH, et al. Engineered heart tissue models from hiPSC-derived cardiomyocytes and cardiac ECM for disease modeling and drug testing applications. *Acta Biomater*. 2019;92:145–159. doi: 10.1016/j.actbio.2019.05.016
21. Ronaldson-Bouchar K, Ma SP, Yeager K, Chen T, Song L, Sirabella D, Morikawa K, Teles D, Yazawa M, Vunjak-Novakovic G. Advanced maturation of human cardiac tissue grown from pluripotent stem cells. *Nature*. 2018;556:239–243. doi: 10.1038/s41586-018-0016-3
22. Tiburcy M, Hudson JE, Balfanz P, Schlick S, Meyer T, Chang Liao M-L, Levent E, Raad F, Zeidler S, Wingender E, et al. Defined engineered human myocardium with advanced maturation for applications in heart failure modeling and repair. *Circulation*. 2017;135:1832–1847. doi: 10.1161/circulationaha.116.024145
23. Ogle BM, Bursac N, Domian I, Huang NF, Menasché P, Murry CE, Pruitt B, Radisic M, Wu JC, Wu SM, et al. Distilling complexity to advance cardiac tissue engineering. *Sci Transl Med*. 2016;8:342ps313. doi: 10.1126/scitranslmed.aad2304
24. Shaheen N, Shiti A, Huber I, Shinnawi R, Arbel G, Gepstein A, Setter N, Goldfracht I, Gruber A, Chorna SV, et al. Human induced pluripotent stem cell-derived cardiac cell sheets expressing genetically encoded voltage indicator for pharmacological and arrhythmia studies. *Stem Cell Rep*. 2018;10:1879–1894. doi: 10.1016/j.stemcr.2018.04.006
25. Shinnawi R, Shaheen N, Huber I, Shiti A, Arbel G, Gepstein A, Ballan N, Setter N, Tijssen AJ, Borggreffe M, et al. Modeling reentry in the short QT syndrome with human-induced pluripotent stem cell-derived cardiac cell sheets. *J Am Coll Cardiol*. 2019;73:2310–2324. doi: 10.1016/j.jacc.2019.02.055
26. Herron TJ, Rocha AMD, Campbell KF, Ponce-Balbuena D, Willis BC, Guerrero-Serna G, Liu Q, Klos M, Musa H, Zarzoso M, et al. Extracellular matrix-mediated maturation of human pluripotent stem cell-derived cardiac monolayer structure and electrophysiological function. *Circ Arrhythm Electrophysiol*. 2016;9:e003638. doi: 10.1161/CIRCEP.113.003638
27. Gruber A, Edri O, Gepstein L. Cardiac optogenetics: the next frontier. *Europace*. 2018;20:1910–1918. doi: 10.1093/europace/eux371
28. Zhang F, Vierock J, Yizhar O, Fenno LE, Tsunoda S, Kianianmomeni A, Prigge M, Berndt A, Cushman J, Polle J, et al. The microbial opsin family of optogenetic tools. *Cell*. 2011;147:1446–1457. doi: 10.1016/j.cell.2011.12.004
29. Iyer SM, Montgomery KL, Towne C, Lee SY, Ramakrishnan C, Deisseroth K, Delp SL. Virally mediated optogenetic excitation and inhibition of pain in freely moving nontransgenic mice. *Nat Biotechnol*. 2014;32:274–278. doi: 10.1038/nbt.2834
30. Nussinovitch U, Shinnawi R, Gepstein L. Modulation of cardiac tissue electrophysiological properties with light-sensitive proteins. *Cardiovasc Res*. 2014;102:176–187. doi: 10.1093/cvr/cvu037
31. Vogt CC, Bruegmann T, Malan D, Ottersbach A, Roell W, Fleischmann BK, Sasse P. Systemic gene transfer enables optogenetic pacing of mouse hearts. *Cardiovasc Res*. 2015;106:338–343. doi: 10.1093/cvr/cvv004
32. Nussinovitch U, Gepstein L. Optogenetics for in vivo cardiac pacing and resynchronization therapies. *Nat Biotechnol*. 2015;33:750–754. doi: 10.1038/nbt.3268
33. Scardigli M, Müllenbroich C, Margoni E, Cannazzaro S, Crocini C, Ferrantini C, Coppini R, Yan P, Loew LM, Campione M, et al. Real-time optical manipulation of cardiac conduction in intact hearts. *J Physiol*. 2018;596:3841–3858. doi: 10.1113/JP276283
34. Bruegmann T, Boyle PM, Vogt CC, Karathanos TV, Arevalo HJ, Fleischmann BK, Trayanova NA, Sasse P. Optogenetic defibrillation terminates ventricular arrhythmia in mouse hearts and human simulations. *J Clin Invest*. 2016;126:3894–3904. doi: 10.1172/JCI88950
35. Crocini C, Ferrantini C, Coppini R, Scardigli M, Yan P, Loew LM, Smith G, Cerbai E, Poggesi C, Pavone FS, et al. Optogenetics design of mechanically-based stimulation patterns for cardiac defibrillation. *Sci Rep*. 2016;6:35628. doi: 10.1038/srep35628
36. Nyns EC, Kip A, Bart CI, Plomp JJ, Zeppenfeld K, Schalij MJ, de Vries AA, Pijnappels DA. Optogenetic termination of ventricular arrhythmias in the whole heart: towards biological cardiac rhythm management. *Eur Heart J*. 2017;38:2132–2136. doi: 10.1093/eurheartj/ehw574
37. Nyns ECA, Poelma RH, Volkers L, Plomp JJ, Bart CI, Kip AM, van Brakel TJ, Zeppenfeld K, Schalij MJ, Zhang GQ, et al. An automated hybrid bioelectronic system for autogenous restoration of sinus rhythm in atrial fibrillation. *Sci Transl Med*. 2019;11:eaau6447. doi: 10.1126/scitranslmed.aau6447
38. Sasse P, Funken M, Beiert T, Bruegmann T. Optogenetic termination of cardiac arrhythmia: mechanistic enlightenment and therapeutic application? *Front Physiol*. 2019;10:675. doi: 10.3389/fphys.2019.00675
39. Majumder R, Feola I, Teplinen AS, de Vries AA, Panfilov AV, Pijnappels DA. Optogenetics enables real-time spatiotemporal control over spiral wave dynamics in an excitable cardiac system. *Elife*. 2018;7:e41076. doi: 10.7554/eLife.41076
40. Watanabe M, Feola I, Majumder R, Jangsangthong W, Teplinen AS, Ypey DL, Schalij MJ, Zeppenfeld K, de Vries AA, Pijnappels DA. Optogenetic manipulation of anatomical re-entry by light-guided generation of a reversible local conduction block. *Cardiovasc Res*. 2017;113:354–366. doi: 10.1093/cvr/cvx003
41. Dempsey GT, Chaudhary KW, Atwater N, Nguyen C, Brown BS, McNeish JD, Cohen AE, Kralj JM. Cardiotoxicity screening with simultaneous optogenetic pacing, voltage imaging and calcium imaging. *J Pharmacol Toxicol Methods*. 2016;81:240–250. doi: 10.1016/j.vascn.2016.05.003
42. Klimas A, Ambrosi CM, Yu J, Williams JC, Bien H, Entcheva E. OptoDyCE as an automated system for high-throughput all-optical dynamic cardiac electrophysiology. *Nat Commun*. 2016;7:11542. doi: 10.1038/ncomms11542
43. Paci M, Passini E, Klimas A, Severi S, Hyttinen J, Rodriguez B, Entcheva E. All-optical electrophysiology refines populations of in silico human

- iPSC-CMs for drug evaluation. *Biophys J*. 2020;118:2596–2611. doi: 10.1016/j.bpj.2020.03.018
44. Dwenger M, Kowalski WJ, Ye F, Yuan F, Tinney JP, Setozaki S, Nakane T, Masumoto H, Campbell P, Guido W, et al. Chronic optical pacing conditioning of hiPSC engineered cardiac tissues. *J Tissue Eng*. 2019;10:2041731419841748. doi: 10.1177/2041731419841748
  45. Lemme M, Braren I, Prondzynski M, Aksehirlioglu B, Ulmer BM, Schulze ML, Ismaili D, Meyer C, Hansen A, Christ T, et al. Chronic intermittent tachypacing by an optogenetic approach induces arrhythmia vulnerability in human engineered heart tissue. *Cardiovasc Res*. 2020;116:1487–1499. doi: 10.1093/cvr/cvz245
  46. Lemoine MD, Lemme M, Ulmer BM, Braren I, Krasemann S, Hansen A, Kirchhof P, Meyer C, Eschenhagen T, Christ T. Intermittent optogenetic tachypacing of atrial engineered heart tissue induces only limited electrical remodelling. *J Cardiovasc Pharmacol*. 2020;77:291–299. doi: 10.1097/FJC.0000000000000951
  47. Dwenger M, Kowalski WJ, Masumoto H, Nakane T, Keller BB. Chronic optogenetic pacing of human-induced pluripotent stem cell-derived engineered cardiac tissues. *Methods Mol Biol*. 2021;2191:151–169. doi: 10.1007/978-1-0716-0830-2\_10
  48. Burridge PW, Matsa E, Shukla P, Lin ZC, Churko JM, Ebert AD, Lan F, Diecke S, Huber B, Mordwinkin NM, et al. Chemically defined generation of human cardiomyocytes. *Nat Methods*. 2014;11:855–860. doi: 10.1038/nmeth.2999
  49. Shinnawi R, Huber I, Maizels L, Shaheen N, Gepstein A, Arbel G, Tijssen AJ, Gepstein L. Monitoring human-induced pluripotent stem cell-derived cardiomyocytes with genetically encoded calcium and voltage-fluorescent reporters. *Stem Cell Rep*. 2015;5:582–596. doi: 10.1016/j.stemcr.2015.08.009
  50. Gruber A, Edri O, Huber I, Arbel G, Gepstein A, Shiti A, Shaheen N, Chorna S, Landesberg M, Gepstein L. Optogenetic modulation of cardiac action potential properties may prevent arrhythmogenesis in short and long QT syndromes. *JCI Insight*. 2021;6:e147470. doi:10.1172/jci.insight.147470
  51. Nussinovitch U, Gepstein L. Optogenetics for suppression of cardiac electrical activity in human and rat cardiomyocyte cultures. *Neurophotonics*. 2015;2:031204. doi: 10.1117/1.NPh.2.3.031204
  52. Yankelson L, Feld Y, Bressler-Stramer T, Itzhaki I, Huber I, Gepstein A, Aronson D, Marom S, Gepstein L. Cell therapy for modification of the myocardial electrophysiological substrate. *Circulation*. 2008;117:720–731. doi: 10.1161/CIRCULATIONAHA.106.671776
  53. De Simone SA, Moyle S, Buccarello A, Dellenbach C, Kucera JP, Rohr S. The role of membrane capacitance in cardiac impulse conduction: an optogenetic study with non-excitabile cells coupled to cardiomyocytes. *Front Physiol*. 2020;11:194. doi: 10.3389/fphys.2020.00194
  54. Funken M, Bruegmann T, Sasse P. Selective optogenetic stimulation of fibroblasts enables quantification of hetero-cellular coupling to cardiomyocytes in a three-dimensional model of heart tissue. *Europace*. 2020;22:1590–1599. doi: 10.1093/europace/euaa128
  55. Frazier DW, Wolf PD, Wharton JM, Tang AS, Smith WM, Ideker RE. Stimulus-induced critical point. Mechanism for electrical initiation of re-entry in normal canine myocardium. *J Clin Invest*. 1989;83:1039–1052. doi: 10.1172/JCI113945
  56. Feola I, Volkens L, Majumder R, Teplenin A, Schaliq MJ, Panfilov AV, de Vries AAF, Pijnappels DA. Localized optogenetic targeting of rotors in atrial cardiomyocyte monolayers. *Circ Arrhythm Electrophysiol*. 2017;10:e005591. doi: 10.1161/CIRCEP.117.005591
  57. Streit J, Kleinlogel S. Dynamic all-optical drug screening on cardiac voltage-gated ion channels. *Sci Rep*. 2018;8:1153. doi: 10.1038/s41598-018-19412-z
  58. Quach B, Krogh-Madsen T, Entcheva E, Christini DJ. Light-activated dynamic clamp using iPSC-derived cardiomyocytes. *Biophys J*. 2018;115:2206–2217. doi: 10.1016/j.bpj.2018.10.018
  59. Park S-J, Zhang D, Qi Y, Li Y, Lee KY, Bezzerides VJ, Yang P, Xia S, Kim SL, Liu X, et al. Insights into the pathogenesis of catecholaminergic polymorphic ventricular tachycardia from engineered human heart tissue. *Circulation*. 2019;140:390–404. doi: 10.1161/CIRCULATIONAHA.119.039711
  60. Bingen BO, Engels MC, Schaliq MJ, Jangsangthong W, Neshati Z, Feola I, Ypey DL, Askar SFA, Panfilov AV, Pijnappels DA, et al. Light-induced termination of spiral wave arrhythmias by optogenetic engineering of atrial cardiomyocytes. *Cardiovasc Res*. 2014;104:194–205. doi: 10.1093/cvr/cvu179

# **SUPPLEMENTAL MATERIAL**

**Figure S1. Plots describing the behavior of the probability of successful rotor termination vs. illumination duration using different illumination grids.**



Notice that the rate of the increase in the probability of rotor termination with the change in illumination duration (slope of the lines) progressively decreases moving from a grid of 25% to 100% grid.

## **Supplemental Video Legends:**

Dynamic displays showing changes in the fluorescent signal over time as derived by optical mapping of a representative hiPSC-CCS. Depolarization appears as darkening of the affected area within the tissue. Video speed is 0.25 of the real-time speed. The visual field is 1cm<sup>2</sup>.

**Video S1. Spiral wave induction by a diffuse optogenetic S1-S2 stimulation protocol.**

**Video S2. Spiral wave induction by the cross-field optogenetic stimulation protocol.**

**Video S3. Spiral wave termination by diffuse illumination.**

**Video S4. Mechanism of unsuccessful optogenetic attempt to terminate a spiral wave by using a prolonged illumination protocol. Note the initial successful rotor termination followed by peripheral depolarization and induction of a new reentrant circuit.** hiPSC-CCSs: human induced pluripotent stem cell-derived cardiomyocyte cell sheets.